bioRxiv preprint doi: https://doi.org/10.1101/798884; this version posted October 11, 2019. The copyright holder for this preprint (which was not certified by peer review) is the author/funder. All rights reserved. No reuse allowed without permission.

FUS-dependent phase separation initiates double-strand break repair

Silvia C. Lenzken[1]$, Brunno R. Levone[1]$, Giuseppe Filosa[1,2], Marco Antonaci[1], Francesca Conte[1*], Cise Kizilirmak[1#], Stefan Reber[3], Alessia Loffreda[1§§], Fabio Biella[1§], Antonella E. Ronchi[1], Oliver Mühlemann[4], Angela Bachi[2], Marc-David Ruepp[3], Silvia M.L. Barabino[1]

[1] Department of Biotechnology and Biosciences, University of Milano-Bicocca, Milan, Italy

[2]Functional Proteomics Program, Istituto FIRC di Oncologia Molecolare (IFOM), Milan, Italy

[3]UK Dementia Research Institute, Institute of Psychiatry, Psychology & Neuroscience, King's College London, London, United Kingdom

[4]Department of Chemistry and Biochemistry, University of Bern, Bern, Switzerland

$These two authors contributed equally to this work.

[*]Present address: Institute of Molecular Biology (IMB)¸ Ackermannweg 4, 55128 Mainz, Germany

[#]Present address: Division of Genetics and Cell Biology, San Raffaele Scientific Institute, Via Olgettina 58, 20132 Milan Italy

[§]Present address: Department of Pathophysiology and Transplantation (DEPT), University of Milan, 20122 Milan, Italy.

[§§]Present address: Experimental Imaging Centre, San Raffaele Scientific Institute, Via Olgettina 58, 20132 Milan Italy

Running title: RNA-binding proteins in DNA repair

Corresponding author: Silvia M.L. Barabino

Department of Biotechnology and Biosciences

University of Milano-Bicocca, Piazza della Scienza, 2

I-20126 Milano, Italy

Phone: +39-02-6448 3352

bioRxiv preprint doi: https://doi.org/10.1101/798884; this version posted October 11, 2019. The copyright holder for this preprint (which was not certified by peer review) is the author/funder. All rights reserved. No reuse allowed without permission.

Summary

RNA-binding proteins (RBPs) are emerging as important effectors of the cellular DNA damage response (DDR). Implicated in RNA metabolism and DNA repair, the RBP Fused-in-sarcoma (FUS) contains a prion-like domain (PLD) and undergoes reversible phase separation. Here, we report that liquid-liquid phase separation (LLPS) occurs at DNA damage foci and is necessary for the efficient recruitment of key DDR factors. We show that FUS co-purifies with the DDR factor KU and with SFPQ, another PLD-containing RBP implicated in DNA repair. Moreover, we demonstrate that FUS is required for 53BP1 localisation to DNA damage foci and for the correct recruitment of KU80 and NBS1 to sites of DNA damage. LLPS-deficient FUS variants impair retention of the DNA damage sensor KU at sites of DNA damage, and the recruitment of SFPQ. These findings provide a mechanistic function for FUS-dependent LLPS in the activation of the DDR and in the recruitment of DDR factors and RBPs at sites of DNA damage.

bioRxiv preprint doi: https://doi.org/10.1101/798884; this version posted October 11, 2019. The copyright holder for this preprint (which was not certified by peer review) is the author/funder. All rights reserved. No reuse allowed without permission.

Introduction

Despite evolution requiring genetic variability, DNA mutations are a threat for the survival of the individual. Unrepaired DNA damage can lead to genome instability, a hallmark of cancer cells. To maintain genome stability and to counteract DNA damage, cells have evolved a complex cellular response, commonly referred to as DNA damage response (DDR). The early DDR events have been best elucidated at sites of DNA double strand breaks (DSBs), which are the most dangerous type of DNA lesions. After occurrence of a DSB, the sensor protein kinases DNA-PK (DNA-dependent protein kinase), ATM (ataxia telangiectasia mutated), and ATR (ATM and Rad3 related) are rapidly activated, and the KU70/KU80 (XRCC6/XRCC5) heterodimer is recruited to the broken DNA ends. Phosphorylation of the histone variant H2AX (known as γH2AX) by ATM serves as an early mark of DNA damage and as a platform for the recruitment of early DDR factors such as MDC1, and the MRN complex (consisting of MRE11, NBS1 and RAD50) (Stucki and Jackson, 2006). In mammalian cells, the accumulation of DDR factors at sites of DNA damage gives rise to subnuclear foci that can be readily visualised microscopically. In mammals, DSBs are eventually repaired via two main pathways depending on the cell cycle phase: homologous recombination (HR) that repairs DSBs in S and G2 phases, and non-homologous end joining (NHEJ), which is active throughout the entire cell cycle.

In addition to these canonical DDR factors, large-scale proteomic and genomic studies have identified several RNA-binding proteins (RBPs) as potential novel DDR factors, either as targets of the apical DDR kinases (Matsuoka et al., 2007) or as proteins that when lost lead to activation of the DDR (Paulsen et al., 2009). RBPs have been shown to contribute both directly and indirectly to genome stability. For example, the loss of pre-mRNA splicing or mRNA export factors can favour the accumulation of RNA:DNA hybrids (R-loops) that can be processed to DSBs (Chuang et al., 2019; Li and Manley, 2005). In addition, an increasing number of studies have shown that several RBPs are recruited to sites of DNA damage and participate in DSB repair (Mikolaskova et al., 2018).

The multifunctional DNA/RNA-binding protein Fused-in-sarcoma (FUS) is involved in splicing, translation, and mRNA transport (Dormann and Haass, 2013). Both *in vivo* and *in vitro* observations point towards a role for FUS in maintaining genome stability. Mice lacking FUS are hypersensitive to ionising radiation (IR), show defects in spermatogenesis, and high levels of chromosomal instability (Hicks et al., 2000; Kuroda et al., 2000). *In vitro*, FUS stimulates the formation of DNA loops (D-loops) between complementary DNA molecules,

bioRxiv preprint doi: https://doi.org/10.1101/798884; this version posted October 11, 2019. The copyright holder for this preprint (which was not certified by peer review) is the author/funder. All rights reserved. No reuse allowed without permission.

structures that correspond to one of the first steps in HR (Baechtold et al., 1999). cells, FUS is recruited very early at sites of DNA damage (Aleksandrov et al., 2018; Mastrocola et al., 2013) and its silencing leads to an impairment of DSB repair both by HR and NHEJ (Mastrocola et al., 2013; Wang et al., 2013). In addition, FUS is an ATM and DNA-PK substrate (Deng et al., 2014; Gardiner et al., 2008).

The N-terminal region of FUS (residues 1–165) is a highly conserved prion-like domain (PLD) composed primarily of serine, tyrosine, glycine, and glutamine (QGSY-rich). This domain mediates protein:protein interactions and drives the aggregation of FUS into protein inclusions (Sun et al., 2011). Several studies have shown that the PLD of FUS undergoes a reversible dynamic phase transition between a disperse state, liquid droplets and hydrogels (Kato et al., 2012; Murakami et al., 2015; Patel et al., 2015). FUS liquid–liquid phase separation (LLPS) occurs both *in vivo* and *in vitro* at physiological concentrations (Burke et al., 2015; Murakami et al., 2015).

It is increasingly recognised that LLPS provides a molecular basis for the formation of subcellular membrane-less organelles such as nucleoli, Cajal bodies, paraspeckles, and stress granules (Boeynaems et al., 2018). Paraspeckles are subnuclear compartments of poorly characterised function that assemble on the lncRNA NEAT1, which induces phase separation of four core RBPs: SFPQ, NONO, FUS and RBM14 (Hirose et al., 2019). Interestingly, all these proteins contain PLDs of variable length (Harrison and Shorter, 2017). The PLDs of FUS and RBM14 are required for *in vitro* phase separation and *in vivo* paraspeckle formation (Hennig et al., 2015). Interestingly, similarly to FUS, also SFPQ, its paralog NONO, and RBM14 are RBPs implicated in DNA repair. SFPQ silencing was reported to render cells sensitive to DNA crosslinking and alkylating agents, and to reduce DSB repair by HR (Rajesh et al. 2011). SFPQ has DNA re-annealing and strand-invasion activity that may lead to the formation of D-loop structures (Akhmedov and Lopez, 2000). In addition, SFPQ, NONO, and RBM14 also promote NHEJ (Bladen et al., 2005; Jaafar et al., 2017; Simon et al., 2017).

Despite all the observations implicating RBPs such as FUS and SFPQ in DNA damage repair, their precise molecular function remains to be fully elucidated. Here, we report that LLPS occurs at DNA damage foci and is necessary for the efficient recruitment of key DDR factors. LLPS is also required for the efficient recruitment of FUS. We show that FUS is required for the efficient retention of the KU80 subunit on damaged DNA, and the correct recruitment of NBS1 and SFPQ. Importantly, we demonstrate that the recruitment of KU80 and of SFPQ is dependent on FUS-induced LLPS. Overall, these findings highlight an

bioRxiv preprint doi: https://doi.org/10.1101/798884; this version posted October 11, 2019. The copyright holder for this preprint (which was not certified by peer review) is the author/funder. All rights reserved. No reuse allowed without permission.

important early role of FUS in the recruitment of key DDR factors and in promoting LLPS at DNA damage sites.

bioRxiv preprint doi: https://doi.org/10.1101/798884; this version posted October 11, 2019. The copyright holder for this preprint (which was not certified by peer review) is the author/funder. All rights reserved. No reuse allowed without permission.

Results

FUS knock-out sensitises human cells to DNA damage and induces R-loop formation

Recent studies reported that siRNA-mediated silencing of FUS leads to an accumulation of transcription-associated DNA damage (Hill et al., 2016).To further characterise the role of FUS in genome stability, we generated HeLa cells in which the FUS gene was knocked-out (FUS-KO) by CRISPR-trap genome editing (Reber et al., 2018). Western blot analysis showed a substantial increase in the level of γH2AX in FUS-KO cells, while in control cells the phosphorylation of H2AX was almost undetectable (Figure 1A). In addition, immunofluorescence analyses revealed that FUS-KO cells show increased formation of γH2AX foci (Figure 1B). Similarly, the knockdown of FUS in SH-SY5Y also increased the levels of γH2AX (Suppl. Figure 1A). These observations suggest that, in the absence of FUS, cells either generate more DNA damage or they repair DNA damage less efficiently. Indeed, HeLa FUS-KO cells, when complemented with exogenous Flag-tagged FUS, displayed a reduced number of γH2AX foci (Suppl. Figure 1B), demonstrating that FUS is essential for the maintenance of a low level of endogenous DNA damage.

In addition, we observed that FUS-KO cells proliferate slower than wild type cells and indeed, cell cycle analysis showed that a significantly higher fraction of FUS-KO cells accumulated in the G2/M phase when compared to wild type cells (Figure 1C and Supp. Figure 1C).

Next, we determined whether the knockout of FUS altered the cells susceptibility to DNA damage by performing clonogenic survival assays with wild type versus FUS-KO HeLa cells after exposure for 18 h to etoposide (ETO), a DNA topoisomerase II inhibitor that causes double strand breaks (DSBs). Given that HeLa FUS-KO are slower to proliferate, the colonies they formed were smaller than wild type colonies. We observed that HeLa FUS-KO were more sensitive to ETO exposure giving raise to fewer colonies than wild type cells (Figure 1D). The increased sensitivity to genotoxic stress of HeLa FUS-KO cells was further confirmed by a cell viability assay (MTT assay, Figure 1E) indicating that FUS contributes to cell viability upon genotoxic stress.

Depletion of RNA biogenesis factors such as SRSF1 and Y14/RBM8A was shown to favour the accumulation of RNA:DNA hybrids (R-loops) and resulted in R-loop-dependent genomic instability (Chuang et al., 2019; Li and Manley, 2005; Wahba et al., 2011). We thus measured R-loop levels in HeLa wild type and FUS-KO cells by confocal microscopy using the S9.6 monoclonal antibody that specifically recognises RNA:DNA hybrids (Boguslawski et

bioRxiv preprint doi: https://doi.org/10.1101/798884; this version posted October 11, 2019. The copyright holder for this preprint (which was not certified by peer review) is the author/funder. All rights reserved. No reuse allowed without permission.

al., 1986). FUS-KO cells showed a 1.5-fold increase in the nuclear S9.6 signal. (Figure 2A). The increase in the R-loop formation was confirmed by dot-blot analysis (Supp. Figure 2A). This observation suggests that the activation of the DDR observed in FUS-KO cells could be, at least in part, due to the processing of the abnormal RNA:DNA hybrids. To test this hypothesis, wild type and FUS-KO cells were transiently transfected with either a plasmid expressing only GFP or RNase H1-GFP. RNase H1 overexpression in FUS-KO cells decreased both the number of γH2AX foci and the intensity of the γH2AX signal (Figure 2B). To confirm these results, we generated HeLa wild type and HeLa FUS-KO cells stably expressing exogenous doxycycline-inducible HA-tagged RNase H1-M27 (here denominated WT/RNH1 and KO/RNH1, respectively). RNase H1-M27 is a mutant RNase H1 which is exclusively expressed in the nucleus due to a lack of the mitochondrial localisation signal (Cerritelli et al., 2003). As the inducible lines showed already a basal expression in the absence of doxycycline, this allowed us to perform the experiments without induction (Supp. Figure 2B), thereby preventing RNase H1 overexpression-induced toxicity, which was observed by others (Shen et al., 2017). The overexpression of RNase H1 in KO/RNH1 cells resulted in a 1.6-fold decrease in R-loops content (Figure 2C), a 1.4-fold reduction in the number of γH2AX foci (Figure 2 D), and in a reduction of H2AX phosphorylation levels (Figure 2E). Overall, these observations suggest that the DNA damage observed in the absence of FUS is due at least in part to the accumulation of R-loops that are processed to DSBs. An alternative possibility, however, is that RNAse H1 is directly involved in DSB repair and thus its overexpression facilitates the repair, similar to what was observed in *Schizosaccharomyces pombe* (Ohle et al., 2016).

FUS knock-out affects ATM-dependent signalling and recruitment of DDR factors

Next, we asked whether FUS could be directly involved in DDR signalling. HeLa wild type and FUS-KO cells were treated with ETO for 1 h and then allowed to recover in ETO-free medium for 2 h (Figure 3A). As expected, Western blot analysis of cell extracts showed an increased phosphorylation of ATM, CHK2, BRCA1, and TRIM28, in addition to increased levels of γH2AX after ETO treatment in both cell lines. However, we observed a persistent phosphorylation of all these proteins after 2 h recovery from the ETO treatment in FUS-KO cells, when compared to WT cells (Figure 3A). These observations show that the activation of the DDR occurs normally in the absence of FUS, but that DNA damage signalling persists longer after the release from the genotoxic treatment. Thus, we concluded that cells lacking FUS either generate more DNA damage than WT cells upon ETO treatment, or they repair the DNA damage much less efficiently, or both.

bioRxiv preprint doi: https://doi.org/10.1101/798884; this version posted October 11, 2019. The copyright holder for this preprint (which was not certified by peer review) is the author/funder. All rights reserved. No reuse allowed without permission.

To further explore the role of FUS in the DDR, we investigated whether the absence of FUS affects the recruitment of DDR factors at sites of DNA damage after 1 h ETO treatment, and after 2 h recovery. As shown in Figure 3B, after 1 h ETO we observed the same number of γH2AX foci in wild type and FUS-KO cells, indicating that the absence of FUS does not prevent the initial sensing of DSBs. However, after 2 h recovery from ETO, FUS-KO cells have more γH2AX foci than wild type cells, which indicates that while wild type cells initiate to repair the DNA damage, FUS-KO accumulates it for longer. Moreover, after 1 h ETO, FUS-KO cells showed significantly less 53BP1 foci than wild type cells. Interestingly, 53BP1 foci formation was restored 2 h after recovery, suggesting that FUS is required very early in the DDR, but its presence is not required at later time points.

To evaluate the impact of FUS depletion on DSB repair we used U2OS cells stably transfected with GFP reporter constructs that allow the measurement of HR and NHEJ-mediated repair (Gunn and Stark, 2012). The constructs are based on an engineered GFP gene containing recognition sites for the I-SceI endonuclease for induction of DSBs. The starting constructs are GFP negative as the GFP gene is inactivated by an additional exon, or by mutations. Successful repair of the I-SceI-induced breaks by NHEJ or HR restores the functional GFP gene. The number of GFP positive cells, as counted by flow cytometry, provides a quantitative measure of the NHEJ or HR efficiency. Depletion of FUS by RNAi affected NHEJ repair in a manner similar to the depletion of KU80, one of the two subunits of the KU heterodimer that binds the broken ends of DNA fragments (Figure 3D). Co-depletion of both proteins resulted in an even stronger impairment of the repair pathway. Depletion of FUS also compromised HR efficiency, similar to the effect seen upon depletion of TOPBP1. Also in this case, the concomitant depletion of both proteins showed an additive effect. These results are consistent with previous reports (Mastrocola et al., 2013; Wang et al., 2013) and highlight an important early role of FUS in DSB repair.

To gain insight in the molecular function of FUS during the early DDR events, we then analysed the recruitment kinetics at DSBs of two apical DDR factors, the 80 kDa subunit of the KU heterodimer, and NBS1, one of the subunits of the MRN complex. WT and FUS-KO cells were transiently transfected with GFP-tagged KU80 or GFP-NBS1 plasmids and were then subjected to laser microirradiation to induce a time-specific and localised DNA damage (Suppl. Figure 3A). Real time recording revealed that, in wild type cells, KU80 reached a peak of recruitment to the site of DNA damage within 5 s after microirradiation, remaining there until the end of the assessment (180 s) (Figure 3E and Suppl. Figure 3B). In FUS-KO cells, KU80 showed similar recruitment kinetics but its accumulation was severely impaired. In

bioRxiv preprint doi: https://doi.org/10.1101/798884; this version posted October 11, 2019. The copyright holder for this preprint (which was not certified by peer review) is the author/funder. All rights reserved. No reuse allowed without permission.

contrast, upon laser microirradiation, NBS1 showed slower recruitment kinetics, reaching a peak after about 130 s from the microirradiation (Figure 3F and Supp. Figure 3C). However, in the absence of FUS, NBS1 was more efficiently recruited when compared to wild type cells.

Finally, we monitored the recruitment of GFP-53BP1, a DDR effector required for NHEJ. Consistent with the delayed appearance of 53BP1 foci in FUS-KO cells upon ETO treatment, the recruitment of GFP-53BP1 was also delayed and reduced (Figure 3G and Supp. Figure 3D). Overall, these observations demonstrate that FUS plays an apical role in DDR activation, in particular in recruitment of KU80 at DNA broken ends. In addition, our results suggest that, when stable KU80 binding is impaired, MRN can more effectively gain access to the DNA ends.

Proteomic characterisation of the FUS interactome

We reported earlier the interactome analysis of FUS (Reber et al., 2016). Interestingly, among the FUS interactors, we noticed a substantial number of proteins that are involved in the DDR according to Gene Ontology (GO) analysis, including PARP1/2, XRCC6/KU70 and XRCC5/KU80. Thus, to clarify the role that FUS exerts in the DDR, we sought to determine whether the interactome of FUS changes upon DNA damage. We applied a label-free quantitative mass spectrometry (MS) approach to identify and relatively quantify FUS-interacting proteins whose binding affinity changes upon ETO treatment. HEK293T cells stably expressing Flag-tagged FUS were treated with 10 μM ETO for 1 h. Two biological replicates of the experiment were performed, and only proteins quantified in both experiments were retained for further analysis. The results of the MS analysis are reported in a volcano plot (Figure 4A). The proteins with a fold change of at least 1.3 and a corrected p-value <0.05 were considered significantly changing in the non-treated and the ETO-treated cells.

Surprisingly, ETO treatment did not enhance the affinity for FUS of most of the DDR-related proteins that we had identified in our original interactome analysis (Reber et al., 2016). From the quantitative analysis, however, we identified a small subset of proteins whose abundance was reduced (Supp. Table 1) and a larger group of interactors, which were more represented in the ETO-treated samples (Supp. Table 2). GO enrichment analysis of this dataset showed a significant enrichment for nucleic acids-binding proteins, and in particular for RNA-binding proteins participating in ribonucleoprotein complexes and pre-mRNA splicing (Figure 4B). Interestingly, some of these RNA-binding proteins are linked to R-loop homeostasis (DHX9, NONO, SFPQ,(Chakraborty et al., 2018; Cristini et al., 2018; Petti et al., 2019)), to the DDR (ILF2, MATR3, NONO, SFPQ, (Marchesini et al., 2017; Salton et al., 2010)) or were

bioRxiv preprint doi: https://doi.org/10.1101/798884; this version posted October 11, 2019. The copyright holder for this preprint (which was not certified by peer review) is the author/funder. All rights reserved. No reuse allowed without permission.

found mutated in ALS (HNRNP A2B1, MATR3, (Chia et al., 2018)). We validated a subset of the interactors by co-immmunoprecipitating endogenous proteins in the presence of RNase A (Figure 4C). Interestingly, in these conditions FUS predominantly interacts with the shorter hnRNP A2 isoform.

To determine whether FUS and a subset of its interactors form distinct complexes we performed size-fractionation chromatography of Flag-FUS immunoprecipitates (Figure 4D). As expected in the context of a Flag-FUS immunoprecipitation, FUS was detected throughout the gradient with peak intensities around its own MW (fractions 18-20) and at very high MW, in fractions 1 and 2 and. In these fractions, FUS is present in a complex containing also DHX9, ILF2, and MATR3. DHX9 and MATR3 co-eluted with FUS also between fractions 11 and 14. The heterodimer SFPQ/NONO was detected in two peaks corresponding to fractions 1-4 and fractions 12-15, thus overlapping with both DHX9 and MATR3 (data not shown and Figure 4E, respectively). In contrast, hnRNP A2/B1 showed a very different distribution (Figure 4D). Two major isoforms of this protein have been described, the large isoform of 37.4 kDa (isoform B1) and the smaller isoform A2 of 36 kDa. While B1 was distributed in fractions 2-6, A2 that was predominantly present in fractions 20-22. Finally, ALY/REF was exclusively present in fractions 16-1 (Figure 4D). These data suggest the presence of at least four distinct types of FUS-containing complexes.

To determine whether the association of FUS with different interactors changed upon genotoxic treatment, we then performed size-fractionation chromatography of Flag-FUS immunoprecipitates prepared from HEK293 cells that had been treated with either vehicle or 10 µM ETO for 1 h. Comparison of the elution profiles showed that DHX9 and XRCC5 were the only two interactors that shifted their distribution upon ETO treatment. DHX9 shifted the peak intensity from fractions 8-10 to fractions 13-15, while XRCC5 shifted to higher MW complexes (Figure 4E).

Finally, we tested if the interaction between FUS and two of the RBPs involved in the DDR (SFPQ and MATR3) could play a functional role in DSB damage repair. To this end, we assessed the effect of a double knockdown on DSB repair using the GFP-reporter constructs described above. The concomitant silencing of FUS and of either MATR3 (Figure 4F) or the SFPQ/NONO heterodimer (Figure 4G) silencing did not show an additive effect suggesting an epistatic relationship between FUS, MATR3 and SFPQ/NONO.

FUS promotes the recruitment of SFPQ to sites of DNA damage

bioRxiv preprint doi: https://doi.org/10.1101/798884; this version posted October 11, 2019. The copyright holder for this preprint (which was not certified by peer review) is the author/funder. All rights reserved. No reuse allowed without permission.

To test whether a hierarchical relationship between FUS and SFPQ in DSB repair exists, we compared SFPQ recruitment to laser-induced DNA damage sites in HeLa wild type and FUS-KO cells (Figure 5A). GFP-SFPQ recruitment kinetics in wild type cells was consistent with what has been reported for the SFPQ/NONO heterodimer (Kuhnert et al., 2012). GFP-SFPQ was first detected approximately 20 s after irradiation and reached a maximum after 100 s then slowly declining (Suppl. Figure 5). Strikingly, the recruitment of SFPQ to DSBs in FUS-KO cells was both severely delayed and impaired. This data reveals that the recruitment of SFPQ to DSB sites is FUS-dependent.

As FUS and SFPQ are both core components of paraspeckles and contain prion-like domains that were shown to liquid:liquid phase separate (LLPS) (Yamazaki et al., 2018), we hypothesised that LLPS could play a role in their recruitment at laser-induced DNA damage sites. We initially tested this hypothesis by exposing HeLa cells to 1,6-hexanediol (1,6-HD), an aliphatic alcohol that is known to dissolve various cytoplasmic and nuclear membrane-less compartments *in vivo* (Kroschwald et al., 2015; Lin et al., 2016; Updike et al., 2011; Yamazaki et al., 2018), and which was shown to partially dissolve FUS polymers *in vitro* (Lin et al., 2016). We incubated HeLa cells transiently transfected with GFP-FUS for 10 minutes with 2% 1,6-HD prior to laser microirradiation. At this concentration, we observed that cells were able to recover their normal morphology 2 h after withdrawal from the alcohol (Supp. Figure 4A) and Cajal Bodies were only partially disrupted, while nuclear speckles were very little affected (as shown by anti-coilin and anti-SC35 staining, Supp. Figure 4B). Hence, 1,6-HD condition used here was mild enough not to disrupt all subcellular structures. As control, we performed the same experiment in the presence of 2% 2,5 hexanediol (2,5-HD) an aliphatic alcohol that does not affect phase-separated structures (Lin et al., 2016). We observed a 1.4x reduction in FUS recruitment upon incubation with 1,6-HD, but not in the presence of 2,5-HD (Figure 5B). This effect was even more dramatic in the case of SFPQ (Figure 5C), in which the recruitment was 4.5x smaller upon 1,6-HD incubation. Overall, these results suggest that LLPS occurs at sites of DNA damage and is required for the efficient recruitment of both FUS and SFPQ.

Since our data suggested that efficient SFPQ recruitment requires FUS, and FUS is able to drive LLPS at low protein concentrations and physiological salt concentrations (Wang et al., 2018), we next asked whether SFPQ recruitment at DNA damage sites is dependent on FUS-induced LLPS. To test this hypothesis, we took advantage of some of the LLPS mutant FUS proteins characterised by Wang and colleagues (Wang et al., 2018). We tested the FUS Y/S (Y →S) and R/K (R→K) variants that strongly affect phase separation, and the FUS Q/G (PLD Q

bioRxiv preprint doi: https://doi.org/10.1101/798884; this version posted October 11, 2019. The copyright holder for this preprint (which was not certified by peer review) is the author/funder. All rights reserved. No reuse allowed without permission.

→G) variant that has instead shown to affect the hardening of droplets (Wang et al., 2018). These FUS proteins were transiently transfected as mCherry fusions in HeLa FUS-KO cells. As shown in Figure 5D, the recruitment at DNA damage sites was very similar for FUS WT and for the FUS Q/G variant. In contrast, the FUS Y/S and R/K variants were significantly less recruited than the FUS WT was.

Next, we tested the effect of the expression of these FUS variants on the recruitment of GFP-SFPQ. To this end, HeLa FUS-KO cells were transiently co-transfected with plasmids expressing GFP-SFPQ and one of the mCherry-FUS proteins (WT, or Y/S, or Q/G, or R/K). As shown in Figure 5E, while complementation of FUS-KO cells with the FUS WT or the FUS Q/G variant was able to rescue SFPQ recruitment, expression of the FUS Y/S variant did not improve SFPQ recruitment at laser induced DNA damage site. Interestingly, in the presence of the R/K variant, SFPQ was initially recruited but was then released from the DSB sites much faster. Overall, these observations implicate a requirement for FUS-driven LLPS for the efficient recruitment and retention of SFPQ at sites of DNA damage. This conclusion is further supported by the observation that FUS recruitment at sites of DNA damage precedes SFPQ (Supp. Figure 5).

Liquid-liquid phase separation is required to maintain the integrity of DNA damage foci

Based on our results, we speculated that the structural basis of DDR foci might involve some form of phase separation. We first tested this hypothesis by exposing HeLa cells to 10 µM ETO with or without 2% 1,6-HD for 30 minutes. After fixation, cells were stained with γH2AX or 53BP1 antibodies to assess DDR foci formation, and with coilin antibody to visualise Cajal bodies (Figure 6A). As shown in Figure 6B and 6C, 2% 1,6-HD treatment severely impaired the formation of γH2AX. In contrast, 53BP1 foci and Cajal bodies were only partially dissolved (Figure 6D). In addition to compromising foci integrity, 1,6-HD treatment also strongly affected DDR signalling, reducing phosphorylation of ATM, H2AX and TRIM28 (Figure 6E).

Next, we sought to determine whether LLPS plays a role in the recruitment of DDR factors at sites of DNA damage. To this end, we first determined the effect of the aliphatic alcohols on the recruitment of GFP-KU80 and GFP-NBS1 (Figure 6F and 6G, respectively) observing a reduction in the recruitment of both DDR factors in the presence of 1,6-HD.

Finally, we tested the effect of the expression of FUS LLPS-deficient variants on the recruitment of KU80. As shown in Figure 6H, while complementation of HeLa FUS-KO cells with WT mCherry-FUS restored efficient retention of KU80, the expression of the FUS variants did not rescue KU80 levels at sites of laser-induced DNA damage. Overall, our data

bioRxiv preprint doi: https://doi.org/10.1101/798884; this version posted October 11, 2019. The copyright holder for this preprint (which was not certified by peer review) is the author/funder. All rights reserved. No reuse allowed without permission.

demonstrate a requirement of FUS-driven LLPS for the stable association of KU80 to DNA damage sites.

Discussion

Although FUS has already been implicated in DNA damage repair (Mastrocola et al., 2013; Singatulina et al., 2019; Wang et al., 2013), its precise molecular function in this process remains to be established. Here, we highlight an important early role of FUS in the recruitment of key DDR factors and in promoting LLPS at DNA damage sites.

To shed light on the multiple biological roles of FUS we generated a HeLa knock-out cell line. We observed that FUS knock-out (FUS-KO) cells display an accumulation of R-loops and a hyperphosphorylation of H2AX, a well-established marker of DSBs. Consistent with these observations FUS KO cells were also arrested in G2/M (Sollier et al., 2014). We and others have reported that FUS plays important functions in transcription and pre-mRNA splicing by binding along the whole length of the nascent RNA (Reber et al., 2016; Rogelj et al., 2012; Yamaguchi and Takanashi, 2016; Yu and Reed, 2015). Thus, similar to other pre-mRNA splicing (Chuang et al., 2019; Li et al., 2005) and 3' end processing factors (Stirling et al., 2012), FUS most likely prevents the aberrant pairing of the nascent RNA to the template DNA strand, thereby reducing the formation of co-transcriptional R-loops that can be processed to DSBs (Sollier et al., 2014). Consistent with this hypothesis we observed that the overexpression of RNase H1 in FUS-KO cells (and the consequent reduction in the accumulation of R-loops) also caused a general reduction in the phosphorylation of H2AX.

Besides accumulating R-loops and basal DNA damage, the knockout of FUS also sensitised cells to genotoxic damage induced by treatment with etoposide (an inhibitor of the topoisomerase II), and inhibited cell proliferation suggesting that FUS could play a direct role in DNA damage repair. This idea was confirmed by the characterisation of the DDR that revealed that FUS-KO cells show a persistent activation of DDR signalling after ETO treatment and delayed the formation of 53BP1 foci.

To shed light on the specific function of FUS in DNA repair, we performed a quantitative mass spectrometry characterisation of FUS interacting proteins in etoposide-treated cells. We identified several DDR factors including KU80. Importantly, we found that FUS is required for the retention of the DSB sensor KU at sites of DNA damage. Interestingly, we observed that in FUS KO cells where retention of KU is impaired, the recruitment of NBS1, one of the three subunits of the MRN complex, was increased by more than 50%. These

bioRxiv preprint doi: https://doi.org/10.1101/798884; this version posted October 11, 2019. The copyright holder for this preprint (which was not certified by peer review) is the author/funder. All rights reserved. No reuse allowed without permission.

observations are consistent with the idea that, due to its high abundance and strong affinity for DNA, KU80 is the first DDR factor that binds to the DNA broken ends irrespective of the cell cycle phase (Shibata et al., 2018). Whenever HR repair is occurring, the KU70/80 heterodimer will be then removed to allow MRN-dependent end resection to occur. Indeed, recent studies provide evidence that KU80 can be removed by the endonucleolytic activity of the MRN complex (Chanut et al., 2016; Myler et al., 2017). Therefore, in the absence of FUS, KU is recruited first but is not efficiently retained so that the MRN complex can successfully compete for the binding to the broken DNA ends. However, this is not sufficient for efficient repair since we and others have demonstrated that the silencing of FUS affects both HR and NHEJ-mediated repair (Figure 4F and 4G (Mastrocola et al., 2013; Wang et al., 2013)).

A further observation that emerged from the MS experiments is that many FUS interactors are RNA-binding proteins with low complexity domains (LC), several of which have already been directly implicated in DNA damage repair (Table 1). The LC domains of RNA binding proteins participate in the formation of liquid-like droplets and in phase separation (Lin et al., 2016; Molliex et al., 2015). Indeed, several of the FUS interactors were shown to phase separate (Wang et al., 2018). Among the FUS interactors previously implicated in DNA damage repair, we found SFPQ. SFPQ belongs to the *Drosophila* behaviour/human splicing (DBHS) protein family together with NONO and PSPC1. DBHS proteins share a common region constituted by two RRMs a conserved region called NonA/paraspeckle domain (NOPS), and a C-terminal coiled-coil domain. In addition, each DBHS protein contains LC sequences of variable length. DBHS proteins are obligatory dimers and can form homo- and heterodimers that can polymerise, forming fibrillary gel-like networks (Lee et al., 2015). SFPQ, NONO and FUS are among the essential components of paraspeckles (Naganuma et al., 2012). Paraspeckles are subnuclear membrane-less organelles that form via the polymerisation of SFPQ and NONO on the lncRNA NEAT1 and the subsequent LLPS induced by the recruitment of FUS and RBM14 (Hirose et al., 2019).

Consistent with a recent report by Pessina et al. we show that LLPS occurs at H2AX foci and is required for activation of the DDR (Pessina et al., 2019). Moreover, our results indicate that FUS, together with SFPQ, contributes to the recruitment of DDR proteins at sites of DNA damage by promoting LLPS. Three lines of evidence support this idea. First, like LLPS-formed Cajal bodies and paraspeckles (Yamazaki et al., 2018), γH2AX foci were sensitive to the aliphatic alcohol 1,6-hexanediol treatment (Figure 6B and 6C). Second, inhibition of LLPS impaired the recruitment of FUS, SFPQ, KU80 and NBS1, and affected DDR signalling (Figure 6D). Third, the absence of FUS or the expression of FUS variants that

bioRxiv preprint doi: https://doi.org/10.1101/798884; this version posted October 11, 2019. The copyright holder for this preprint (which was not certified by peer review) is the author/funder. All rights reserved. No reuse allowed without permission.

do not phase separate impaired the recruitment of SFPQ (Figure 5E) and of KU80 (Figure 6H). The idea that KU, FUS and SFPQ/NONO form a complex is supported by several recent reports (Abbasi and Schild-Poulter, 2018; Morchikh et al., 2017).

Based on these observations, we propose that FUS accumulates at DSBs and undergoes LLPS. The concomitant presence of active RNA polymerase II and newly transcribed RNA suggested by other studies (Francia et al., 2012; Michelini et al., 2017; Ohle et al., 2016; Pessina et al., 2019) could stimulate this transition. Phase-separated FUS subsequently recruits SFPQ/NONO and possibly other RBPs stabilising the binding of the KU heterodimer at DNA damage sites.

bioRxiv preprint doi: https://doi.org/10.1101/798884; this version posted October 11, 2019. The copyright holder for this preprint (which was not certified by peer review) is the author/funder. All rights reserved. No reuse allowed without permission.

Methods

Cell lines, cell culture and treatments

HEK293T cells stably expressing Flag-tagged FUS and HeLa FUS-KO are described in (Reber et al., 2016). U2OS cells stably expressing HR and NHEJ repair reporter were a kind gift J.M. Stark and are described in (Gunn and Stark, 2012). HeLa WT RNASEH1 and HeLa FUS-KO RNASEH1 lines were generated by lentiviral infection with TetO-RNASEH1-M27-HA-IRES-GFP in which the RNase H1-M27 gene is under the control of an inducible tet-ON system and is in frame with an HA tag. All cell lines were tested for mycoplasma contamination and negative.

Cells were cultured in Dulbecco's Modified Eagle's Medium (DMEM High Glucose, Euroclone) supplemented with 10% Foetal Bovine Serum (EuroClone), 2 mM L-Glutamine (EuroClone) 100 IU/ml Penicillin (Euroclone) and 0.1 mg/ml Streptomycin (Euroclone); cells were growth at 37°C and 5% of CO_2. The cell lines transduced with the inducible expression system were cultured in the same conditions but certified Tetracycline-free FBS (Euroclone) was used in order to avoid activation of RNase H1 expression.

Etoposide treatment (ETO) was performed for 1 h with 10 µM diluted in DMSO (Enzo Lifesciences). Where specified, cells were treated with either 2% 1,6-Hexanediol (1,6-HD, diluted in growth medium, Sigma-Aldrich) or 2% 2,5-Hexanediol (2,5-HD, diluted in growth medium, Sigma Aldrich) for 30 minutes.

Plasmid DNA was transfected using Lipofectamine 2000 (Invitrogen) while for siRNA transfection Lipofectamine RNAiMAX (Invitrogen) was used, according to the manufacturer's instructions. The synthetic siRNAs used in this study were purchased from Riboxx Life Sciences GmbH (Germany).

Cell cycle analysis

To determine cell-cycle distribution, cells were fixed with ice-cold 70% ethanol, incubated for 2 h with RNase A (250 µg/ml) and propidium iodide (10 µg/ml) at room temperature and analysed by flow cytometry using a CytoFLEX (Beckman Coulter).

Clonogenic Assay

100 wild type and HeLa FUS-KO cells were seeded per well in a 6-wells plate. After attachment, cells were treated with increasing concentrations of etoposide (DMSO, 0.1, 1, 10, 100 µM) for 18 h. After etoposide removal, cells were allowed to proliferate for 7 days, fixed

bioRxiv preprint doi: https://doi.org/10.1101/798884; this version posted October 11, 2019. The copyright holder for this preprint (which was not certified by peer review) is the author/funder. All rights reserved. No reuse allowed without permission.

and stained with crystal violet (Sigma-Aldrich) in 20% methanol for 2 h. The number of cell colonies was counted using an inverted bright field microscope.

MTT Assay

HeLa WT and FUS-KO cells were seeded at a concentration of 8 x 10^3 cells/well in 96-wells plates. Cells were allowed to attach and were then treated with increasing concentrations of etoposide (DMSO, 0.1, 1, 10, 100 µM) for 18 h. The medium was then replaced with a solution of MTT (3-(4,5-dimethylthiazol-2-yl)-2,5-diphenyltetrazolium bromide; Sigma-Aldrich) to a final concentration of 50 µg/ml in culture medium. Cells were incubated with the MTT solution for 4 h. The MTT solution was then removed and cells were lysed in 100 µl DMSO before reading the absorbance using a multiwell VictorX spectrophotometer (Perkin-Elmer).

DNA constructs

The lentiviral expression vector encoding the C-terminally HA tagged-RNASEH1 was generated as follows: annealed and phosphorylated oligonucleotides encoding BsmBI – BamHI restriction sites and 6 x GLY linker-HA tag followed by the stop codon TAG were cloned into the pGEM-T Easy vector to create *pGEM polylinker-HA* vector. RNASEH1-M27 encoded in the pEGFP-M27-H1 vector (a gift from Dr S Cerritelli, NIH, Bethesta, USA) was PCR amplified and was cloned into the BsmBI and BamHI sites of the *pGEM polylinker-HA* to create pGEM-RNASEH1-M27-HA vector. Finally, the fragment containing RNASEH1-M27-HA was isolate by digesting with EcoRI and cloned into the TetO-IRES-GFP vector (a gift from Dr A Zippo, INGM, Milan-Italy) to create TetO-RNASEH1-M27-HA-IRES-GFP. The final vector was verified by restriction digestion and sequencing with Sanger method. NBS1-GFP was kindly provided by Dr. Nussenzweig (Kruhlak et al., 2006). KU80-EGFP was purchased from AddGene. pEGFP-M27-H1 was kindly provided by Dr. S. Cerritelli (Cerritelli et al., 2003). SFPQ-EGFP was generated by subcloning the SFPQ ORF obtained from the Myc-PSF-WT plasmid (Addgene). The FUS-EGFP plasmid was generated by the FUS ORF into pcDNA6F-EGFP. FUS-mCherry plasmids (WT, RK, YS and QG) were kindly provided by Dr.S. Alberti (Wang et al., 2018). All oligonucleotides used in this study are listed in the Supplementary Table 3.

Immunoprecipitations and Immunoblotting

For co-immunoprecipitation, all steps were carried out at 4°C. Lysis were performed with a Mild Buffer 150 (25mM Tris-HCl pH 7.5, 150mM NaCl, 1mM EDTA, 0.5% NP-40, 2.5% Glycerol) for 30min, then the lysate were centrifuged for 15 min at 16,100g and the supernatant

bioRxiv preprint doi: https://doi.org/10.1101/798884; this version posted October 11, 2019. The copyright holder for this preprint (which was not certified by peer review) is the author/funder. All rights reserved. No reuse allowed without permission.

was recovered and quantified by BCA (according to manufacturer protocol). Then, 1 mg of proteins were diluted in Mild Buffer 0 (25 mM Tris-HCl pH 7.5, 1 mM EDTA, 0.5% NP-40, 2.5% Glycerol) to a final concentration of 100 mM NaCl. The lysate was pre-cleaned with 200 µl Protein A Sepharose (GE Healthcare) for 1:30 h on wheel. The pre-cleaned lysate was incubated with the primary antibody on wheel for 1 h and incubated with 200 µl of Protein A Sepharose for further 2 h. Samples were eluted with Laemmli Buffer and fractionated on SDS-PAGE. Quantification of western blots was performed by using the ImageLab software (ChemiDoc, BioRad). Antibodies used in the study are listed in Supplementary Table 4.

Immunofluorescence

Cells were fixed with PFA 4% at RT for 15 min and, after 3 washes with PBS, permeabilised with Triton-X100 0.25% for 5 min. Permeabilised cells were blocked in blocking solution (20% FBS, 0.05% Tween in PBS) for 1 h. Primary antibodies were appropriately diluted in wash buffer (0.2% BSA in PBS) and incubated for 1 h. After 3 washes with wash buffer, cells were incubated with the respective secondary antibodies (diluted in wash buffer) for 1 h. After 3 washes with wash buffer, cells were counterstained with DAPI (Sigma Aldrich) diluted in PBS for 10 min. Coverslips were washed and mounted onto microscope slides using an antifade mounting medium (FluorSave, Calbiochem). For S9.6 staining, cells were fixed with ice-cold methanol (for 10 min at -20°C) and, after 3 washes with PBS, permeabilised with acetone for 1 min. Permeabilised cells where blocked with 3% BSA, 0.1% Tween and 4X SSC Buffer in water for 1 h. Primary antibodies (α-S9.6 and α-Nucleolin) were diluted in blocking solution and cells were incubated at RT for 1:30 h. After 3 washes in wash buffer, cells were incubated in secondary antibodies (diluted in blocking solution) for 1 h. After 3 washes in wash buffer, cells were counterstained with DAPI and mounted onto slides as described above. All antibodies used in the present study are listed in Supplementary Table 4.

Imaging and quantification

Cell imaging was performed using a confocal microscope ECLIPSE - Ti A1 (Nikon). Between 6-10 images were taken per coverslip, using the 60x objective. Quantification of DNA damage foci (γH2AX, 53BP1), subnuclear bodies (Cajal bodies and nuclear speckles) and fluorescence intensity (S9.6) was performed using the software Fiji ImageJ 2.0. At least 130 cells were counted per experiments, which were done in duplicates.

bioRxiv preprint doi: https://doi.org/10.1101/798884; this version posted October 11, 2019. The copyright holder for this preprint (which was not certified by peer review) is the author/funder. All rights reserved. No reuse allowed without permission.

Laser microirradiation

HeLa WT and/or FUS-KO cells were transiently transfected with the appropriated GFP or mCherry-tagged plasmids two days before the irradiation. The following day, transfected cells were plated onto 35 mm plates with a glass bottom and allowed to attach overnight. 30min prior to irradiation, the cell medium was replaced by a phenol red-free medium, containing 0.5 µg/ml of Hoechst (Sigma-Aldrich). Three images were taken as baseline (pre-irradiation) and then cells were irradiated for 4 s using the 405 nm laser at 25% power. The fluorescence intensity of the irradiated area and of two other nuclear regions of interest (ROIs) and one background ROI were assessed. The protein recruitment to the irradiated area was analysed by removing the background fluorescence intensity from each of the other ROIs, then calculating the percentage change at each time point from the average of the three baseline images (pre-irradiation). Finally, the difference between the fluorescence signal in the irradiated region and the average of the two control regions in the nucleus was calculated. The formula used to calculate the protein recruitment is: Recruitment (%) = % from baseline in irradiated ROI – [(% from baseline in control ROI 1 + % from baseline in control ROI 2) / 2]. All the microirradiation experiments were performed using the confocal microscope ECLIPSE - Ti A1 (Nikon). Experiments were done in duplicate and 10 cells were assessed per experiment (to a total of 20 cells per group).

Immunoprecipitations for mass-spectrometric analysis

For mass spectrometry, etoposide-treated and control HEK293T FUS-Flag cells were lysed for 10 min on ice with hypotonic gentle lysis buffer (10 mM Tris-HCl pH 7.5, 10 mM NaCl, 2 mM EDTA, 0.1% Triton X-100, 1x Halt Protease Inhibitor, 1x Phosphatase Inhibitors), followed by supplementation of NaCl to a final concentration of 150 mM, and further incubation on ice for 5 minutes. For the interactome analysis, 10 mM $MgCl_2$ was added together with Benzonase 0.25 U/µl. The cleared lysates were incubated with anti-flag™ M2 Affinity Gel (Sigma Aldrich) for 1.5 h head over tail at 4 °C. The pellet was washed with NET-2 (50 mM Tris-HCl pH 7.5, 150 mM NaCl, 0.05% Triton-X-100) and eluted with the elution buffer (NET-2, 1x protease inhibitor, 1 mg/ml flag peptide).

Label-free Mass Spectrometry and size-exclusion chromatography

Proteins eluted from flag-matrix were digested in-solution with Lys-C and Trypsin using the FASP protocol (Filter Aided Sample Preparation, (Wisniewski, 2017)), with spin ultrafiltration units of nominal molecular weight cut off of 10 kDa. The resulting peptide mixture was purified from the excess of salt and concentrated as previously described (Rappsilber et al., 2007). Mass

bioRxiv preprint doi: https://doi.org/10.1101/798884; this version posted October 11, 2019. The copyright holder for this preprint (which was not certified by peer review) is the author/funder. All rights reserved. No reuse allowed without permission.

spectrometry analysis was performed by nano-liquid chromatography–tandem MS (nLC–ESI-MS/MS). Peptides separation was achieved on a linear gradient from 95% solvent A (2% ACN, 0.1% formic acid) to 40% solvent B (80% acetonitrile, 0.1% formic acid) over 1:30 h and from 40% to 100% solvent B in 2 min at a constant flow rate of 250 nl/min on UHPLC Easy-nLC 1000 (Thermo Scientific) using high pressure bomb loader. MS data were acquired using a data-dependent top10 method for HCD fragmentation. Survey full scan MS spectra (300–1750 Th) were acquired in the Orbitrap with 70000 resolution, AGC target 1e6, IT 120ms. For HCD spectra resolution was set to 35000, AGC target 1e5, IT 120ms; normalised Collision energy 25% and isolation width 3.0 m/z. Three technical replicates of each sample were injected. Raw data files were analysed with Andromeda (MaxQuant software environment version 1.5.2.8u) (Cox et al., 2011) using the following parameters: uniprot_cp_hum_2015_03 as protein database; oxidation (M) and Acetyl (Protein N-term) as variable modifications; carbamidomethyl (C) as fixed modifications; peptide false discovery rate (FDR) 0.01; maximum peptide posterior error probability (PEP) 1; protein FDR 0.01; minimum peptides 2, at least 1 unique; minimum length peptide 7 amino acids; trypsin specificity with up to 2 missed cleavages allowed. The lists of identified proteins were filtered to eliminate reverse hits and known contaminants. A minimum LFQ ratio count of two was considered and the "LFQ intensities". Only proteins identified in both replicates were selected for further analysis. Statistical t-test analysis was performed using Perseus (version 1.5.1.6). For the statistical significance a Benjamini-Hochberg FDR of 0.05 was applied with a permutation test (500 randomisations).

For the size-exclusion chromatography, a separate immunoprecipitation was performed on protein lysates of HEK293T FUS-Flag cells treated and not treated with Etoposide; both treatment and immunoprecipitation were performed in same condition described above. The eluates were loaded in SuperoseTM 6 10/300 GL (GE Healthcare) gel-filtration column, installed on an AKTA FPLC system (GE Healthcare). The column was equilibrated with NET-2 buffer (50 mM Tris-HCl pH 7.5, 150 mM NaCl, 0.05% Triton-X-100), and protein complexes were eluted from the column, using same buffer, at a maximum flow rate of 0.5 ml/min. Approximately 30 fractions were collected for the two immunoprecipitations (ETOP and DMSO), and each separate fraction was concentrated to a final volume of 50 µl with YM-10 Microcon filters (Millipore), reducing SDS-PAGE loading buffer was added and protein samples heat-denatured before Western blotting analysis.

HR and NHEJ repair reporter assays

bioRxiv preprint doi: https://doi.org/10.1101/798884; this version posted October 11, 2019. The copyright holder for this preprint (which was not certified by peer review) is the author/funder. All rights reserved. No reuse allowed without permission.

DSB repair assays were performed in DR-GFP or EJ5-GFP U2OS cell lines (Gunn and Stark, 2012). Briefly, cells were transfected with siRNAs. Two days later cells were co-transfected with a plasmid expressing I-SceI (pCBA-I-SceI) together with appropriates siRNAs using Lipofectamine 2000 (Invitrogen). Cells were harvested after three days post transfection and subjected to flow cytometric analysis to identify and quantify GFP-positive cells (BD FACS Calibur, CellQuest software). The repair efficiency was scored as the percentage of GFP-positive cells; all data were normalised with a control siRNA treatment in each individual experiment.

Statistical analysis

Bar graphs show average ± S.E.M., while boxplot represent median and quartiles (mean is represented by an x). Statistical analysis was performed using the software IBM SPSS Statistics Version 25. Comparison of two groups was done by Student's t-test, while more groups where compared by one-way ANOVA. Two variable comparisons were performed using two-way ANOVA. All post hoc analysis, when necessary, were done using Bonferroni test. Values of $p<0.05$ were considered significant. Significant values are shown by * $p<0.05$, ** $p<0.001$ and *** $p<0.001$.

Acknowledgments

This work was partially supported by the Swiss National Fond Sinergia grant no. CRSII3_136222, the UK Dementia Research Institute, and the NOMIS Foundation. We are grateful to J. Stark for the U2OS cell lines stably expressing HR and NHEJ repair reporters. We are in debt to J. Wang and S. Alberti for having shared their FUS constructs, to S. Cerritelli for having provided the pEGFP-M27-H1 plasmid, and to A. Zippo for having supplied vectors to perform lentiviral infections. NBS1-GFP was kindly provided by A.Nussenzweig.

Data and software availability

The accession number for the mass spectrometry interactome reported in this paper is PRIDE: PXD015232. Link will be accessible upon paper acceptance.

Authors Contribution

S.C.L. conceived and performed the experiments and the data analysis for Figs. 1, 2, 3, 4, 6, and associated supplementary data, and participated in preparing figures and tables. B.R.L.

bioRxiv preprint doi: https://doi.org/10.1101/798884; this version posted October 11, 2019. The copyright holder for this preprint (which was not certified by peer review) is the author/funder. All rights reserved. No reuse allowed without permission.

conceived and performed the experiments and the data analysis for Figs. 1, 2, 3, 5, 6, and associated supplementary data, and participated in preparing figures and tables. G.F. performed all mass spectrometry experiment, the experiments in Fig. 4, and participated in preparing figures and tables, M.A. performed the experiments in Fig. 1A, 2E, 3A, 4C, and 6E and associated supplementary data. F.C. generated the RNASE H1 overexpressing cell lines and performed the experiments in Fig. 1A, 3A and 4C and associated supplementary data. C.K. set up the IF protocol to quantify R-loops and performed the experiments in Fig 1B and 2A. S.R. generated knockout lines and FUS constructs. A.L. performed the experiments in Fig 2B. F.B. participated in the characterisation of the RNASE H1 overexpressing cell lines. A.B. supervised the mass spectrometry analysis and revised the manuscript. A.E.R., O.M., and M.-D.R. critically revised the manuscript. S.M.L.B. conceived the study and wrote the manuscript. All co-authors provided discussion and data interpretation and contributed to the final version of the manuscript.

bioRxiv preprint doi: https://doi.org/10.1101/798884; this version posted October 11, 2019. The copyright holder for this preprint (which was not certified by peer review) is the author/funder. All rights reserved. No reuse allowed without permission.

Figures and Tables

Table 1. **LCD-containing FUS interactors.**

The table was compiled from Naganuma T, Nakagawa S, Tanigawa A, Sasaki YF, Goshima N, Hirose T. EMBO J. 2012 e Henning et al JBC2015

Gene Name	Uniprot Identifier	Repeats in PLD	DDR involvement
HNRNPA1	P09651	2 x [G/S]Y[G/S]	
HNRNPF	P52597	2 x YXXQ, 5 x [S/G]Y[S/G}	
HNRNPH1	P31943	7 x [G/S]Y[G/S]	
HNRNPH3	P31942	6 x [G/S]Y[G/S]	
HNRNPK	P61978	2 x [G/S]Y[G/S]	(Moumen et al., 2013)
HNRNPR	O43390	1 x YNQ, 1 x YGQQ	(Sui et al., 2015)
HNRNPUL1	Q9BUJ2	8 x YXQ, 8 x [G/S]Y[G/S]	(Harrison and Shorter, 2017; Polo et al., 2012)
MATR3	P43243		(Salton et al., 2010)
RBM14	Q96PK6	19 x Y[G/N/A/S]AQ, 2 x [S/G]YG	(Simon et al., 2017)
SFPQ	P23246	1 X SYQ	(Rajesh et al., 2011; Salton et al., 2010)
TAF15	Q86X94	12 x [G/S]Y[G/S], 9 x Y[G/S]Q	

bioRxiv preprint doi: https://doi.org/10.1101/798884; this version posted October 11, 2019. The copyright holder for this preprint (which was not certified by peer review) is the author/funder. All rights reserved. No reuse allowed without permission.

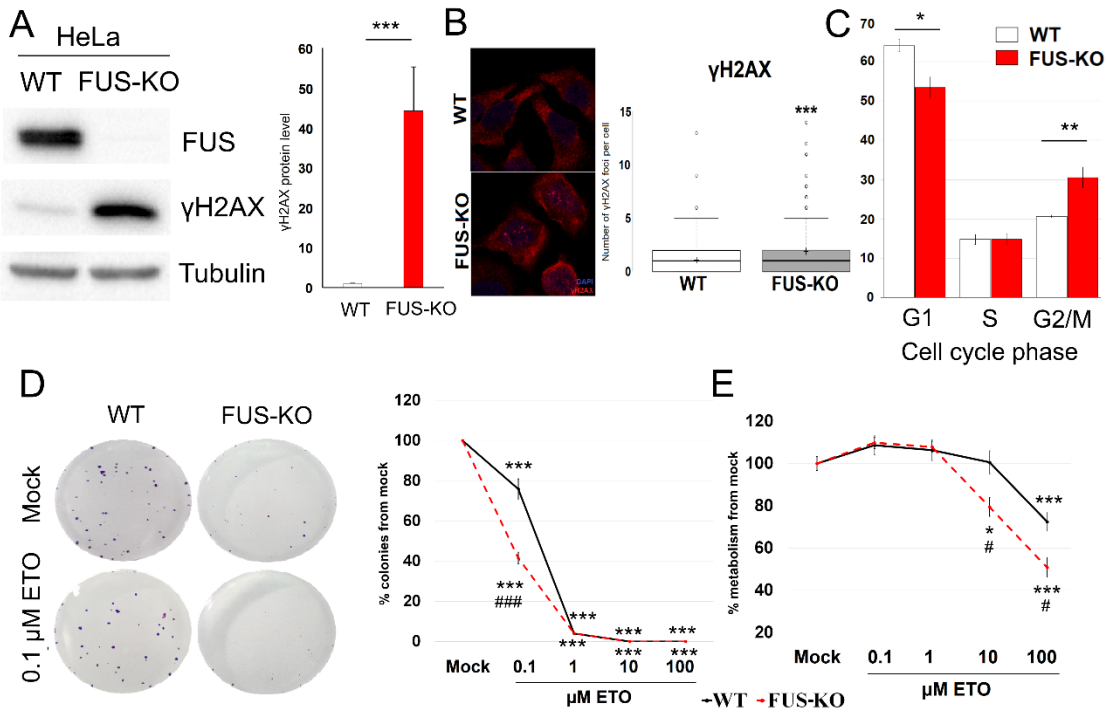

Figure 1. **FUS is required for survival after DNA damage**.

A. Western blots were probed with anti-FUS and anti-γH2AX antibodies and anti-tubulin as loading control. *Left panel*: Representative Western blot; *right panel*: quantification of γH2AX protein level in three independent biological replicates. Statistical significance was determined using Student's t-test (*** p<0.001).

B. *Left panel*: representative confocal images of γH2AX foci in wild type and HeLa FUS-KO cells. Nuclei are stained with DAPI. *Right panel*: Foci quantification; the number of foci per nucleus was counted using the ImageJ software and was plotted as the average number of γH2AX foci per nucleus. Data from two biological replicates, with 170 cells per replicate. Statistical testing was performed using Student's t-test (*** p<0.001).

C. Cell cycle distribution of wild type and HeLa FUS-KO cells. Data represent the average of three independent experiments ± SEM. Statistical significance was determined by Student's t-test (* p< 0.05; **p<0.01).

D. Clonogenic assays were performed to assess the colony formation efficiency of wild type and HeLa FUS-KO cells treated with the indicated ETO concentrations for 18 h and then allowed to proliferate for 7 days. *Left panel*: representative plates stained with crystal violet; *right panel*: bar-chart that represents the average of three independent experiments ± SEM. Statistical significance was determined by two-way ANOVA, which revealed a significant difference between cell lines ($F_{1,20}$=34.9, p<0.001), ETO concentrations ($F_{4,20}$=12248.35, p<0.001) and an interaction between cell lines and ETO concentrations ($F_{4,20}$=356.23, p<0.001). Post-hoc analysis was performed using Bonferroni test (*** p<0.001 in relation to its own mock; ### p<0.001 in relation to WT treated with the same concentration).

E. MTT assay was performed after 18 h treatment with the indicated ETO concentrations. The graph represents the average of three independent experiments ± SEM. Statistical significance was determined

bioRxiv preprint doi: https://doi.org/10.1101/798884; this version posted October 11, 2019. The copyright holder for this preprint (which was not certified by peer review) is the author/funder. All rights reserved. No reuse allowed without permission.

by two-way ANOVA, which revealed a significant difference between cell lines ($F_{1,80}$=9.55, p=0.003), ETO concentrations ($F_{4,80}$=6769.15, p<0.001) and an interaction between cell lines and ETO concentrations ($F_{4,80}$=673.9, p=0.003). Post-hoc analysis was performed using Bonferroni test (* p<0.05, *** p<0.001 in relation to its own mock; # p<0.05 in relation to WT treated with the same concentration).

bioRxiv preprint doi: https://doi.org/10.1101/798884; this version posted October 11, 2019. The copyright holder for this preprint (which was not certified by peer review) is the author/funder. All rights reserved. No reuse allowed without permission.

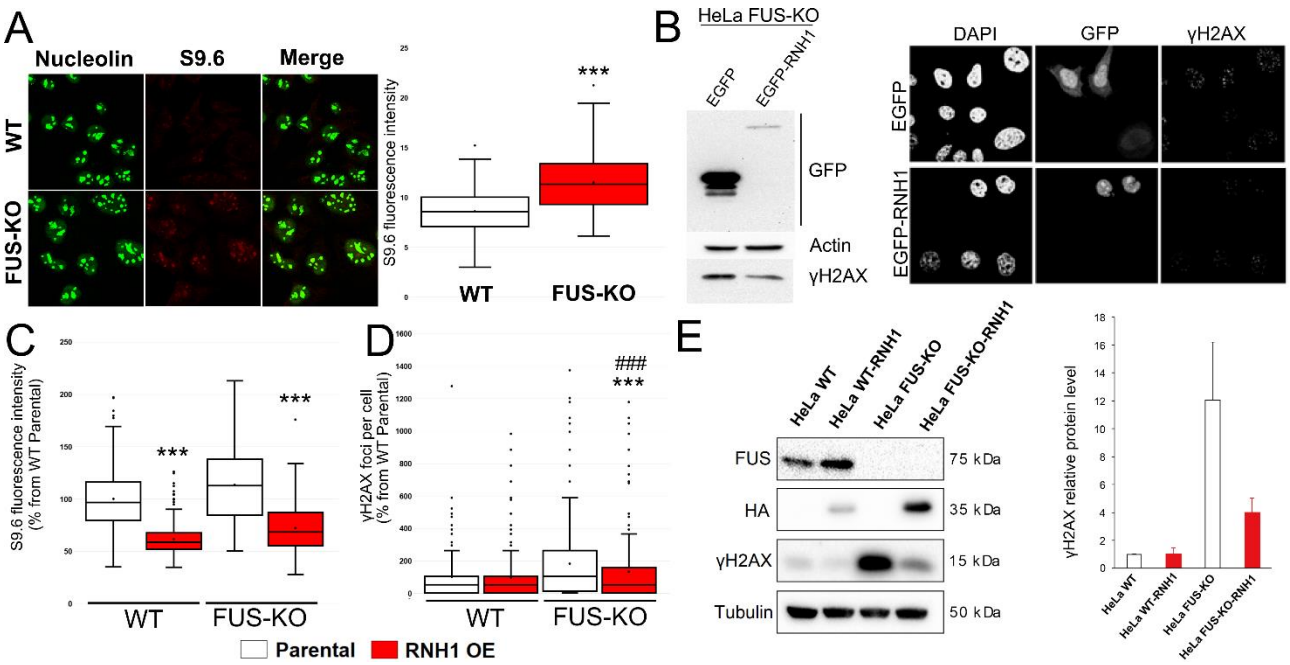

Figure 2. **FUS-KO cells accumulate RNA:DNA hybrids**.

A. *Left panel*: Immunostaining with S9.6 (red) and anti-nucleolin (green) antibodies in HeLa cells. Scale bar represents 10 µm. *Right panel*: Quantification of S9.6 signal shown as box and whiskers plot. Nuclear R-loops were quantified after subtraction of the nucleolar signal (nucleolin staining) as described in Sollier et al. (Sollier et al., 2014). Statistical significance was determined using Student's t-test (*** $p<0.001$).

B. *Left panel*: Western blot analysis of HeLa FUS-KO cell transiently transfected with a plasmid expressing either EGFP or EGFP-RNase H1 probed with anti-GFP and anti-γH2AX antibodies. Anti-actin was used as loading control. *Right panel*: Immunostaining with anti-γH2AX and anti-GFP antibodies.

C. Quantification of the S9.6 nucleoplasmic signal in the parental (either WT or FUS-KO) and in the RNAse H1-M27 expressing lines. Statistical significance was determined using Student's t-test (*** $p<0.001$).

D. Quantification of γH2AX foci as in panel C. Statistical testing was performed using Students t-test (*** $p<0.001$ in relation to FUS-KO Parental; ### $p<0.001$ in relation to WT RNase H1).

E. *Left panel*: Western blot analysis of γH2AX in HeLa cells stably expressing exogenous RNase H1. *Right panel*: quantification of γH2AX foci in the same cell lines.

bioRxiv preprint doi: https://doi.org/10.1101/798884; this version posted October 11, 2019. The copyright holder for this preprint (which was not certified by peer review) is the author/funder. All rights reserved. No reuse allowed without permission.

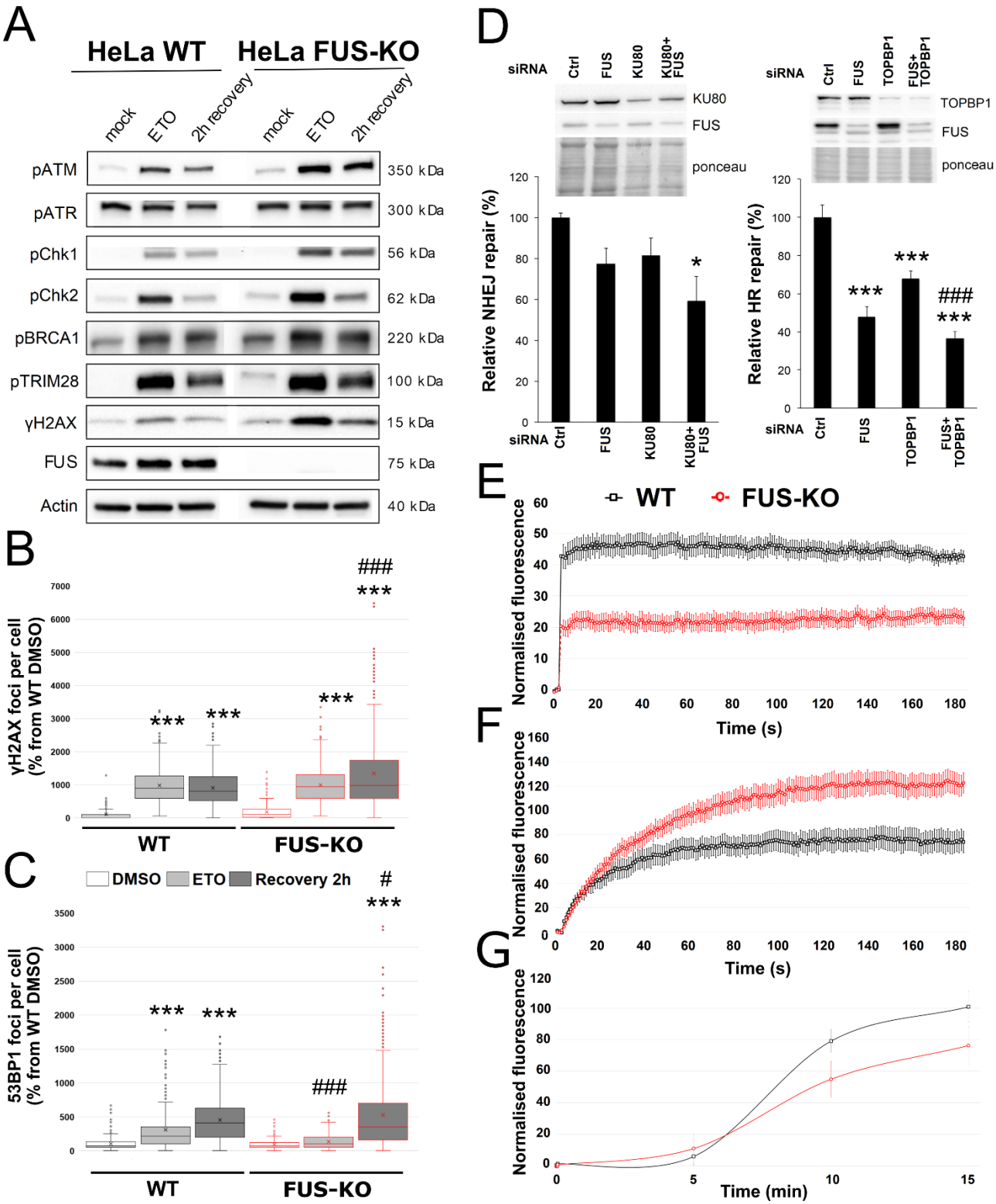

Figure 3. **FUS-KO cells show an impairment in the DDR**.

A. Western blot analysis of DNA Damage repair proteins in HeLa WT and FUS-KO cells treated with ETO for 1 h, and then let to recover in ETO-free media for 2 h. Anti-actin was used as loading control.

B. Immunofluorescence analysis of γH2AX foci upon 1 h ETO treatment and after 2 h recovery. Statistical analysis was performed by two-way ANOVA, which revealed a significant effect of the cell line

bioRxiv preprint doi: https://doi.org/10.1101/798884; this version posted October 11, 2019. The copyright holder for this preprint (which was not certified by peer review) is the author/funder. All rights reserved. No reuse allowed without permission.

($F_{1,2034}$=43.37, p<0.001), of ETO treatments ($F_{2,2034}$=524.34, p<0.001) and an interaction between cell line and ETO treatments ($F_{2,2034}$=23.85, p<0.001). Data analysis was followed by Bonferroni post-hoc tests when appropriated. ***p<0.001 in relation their respective DMSO; ###p<0.001 in relation to the same concentration in HeLa WT cells.

C. Immunofluorescence analysis of 53BP1 foci as in Panel B. Statistical analysis was performed by two-way ANOVA, which revealed a significant effect of the cell line ($F_{1,2034}$=7.01, p=0.008), of ETO treatments ($F_{2,2034}$=311.78, p<0.001) and an interaction between cell line and ETO treatments ($F_{2,2034}$=30.95, p<0.001). Data analysis was followed by Bonferroni post-hoc tests when appropriated. *** p<0.001 in relation their respective DMSO; # p<0.05, ### p<0.001 in relation to the same concentration in HeLa WT cells.

D. DSBs repair efficiency was quantified in U2OS cells containing a stably integrated NHEJ (*left panel*) or a HR (*right panel*) reporter system. Data are presented as the mean ± SEM (n>3). Statistical significance was assessed by one-way ANOVA, which revealed a significant difference in the repair by HR ($F_{3,27}$=30.03, p<0.001) and by NHEJ ($F_{3,12}$=4.04, p=0.034). Bonferroni post hoc test was used for pairwise comparisons. *p<0.05; ***p<0.001 are related to siCtrl; while ### p<0.001 corresponds to comparison with silencing of TOPBP1 alone.

E. WT HeLa and HeLa FUS-KO cells were transiently transfected with GFP-KU80 expressing plasmids. Cells were subjected to laser microirradiation (405 laser) followed by live cell imaging using confocal microscopy. Curve graphs show fluorescence intensities of GFP-fusion proteins at the irradiated region that were quantified periodically (1 measurement per second for 180 s), normalised and presented as mean +/- SEM for 10 cells in each experiment. Experiments were performed in duplicate.

F. WT HeLa and HeLa FUS-KO cells were transiently transfected with a GFP-NBS1 expressing plasmid and subjected to laser microirradiation as in E (1 measurement per second for 180 s).

G. WT HeLa and HeLa FUS-KO cells were transiently transfected with a GFP-53BP1 expressing plasmid and subjected to laser microirradiation as in E (1 measurement every 5 minutes for 15 min).

bioRxiv preprint doi: https://doi.org/10.1101/798884; this version posted October 11, 2019. The copyright holder for this preprint (which was not certified by peer review) is the author/funder. All rights reserved. No reuse allowed without permission.

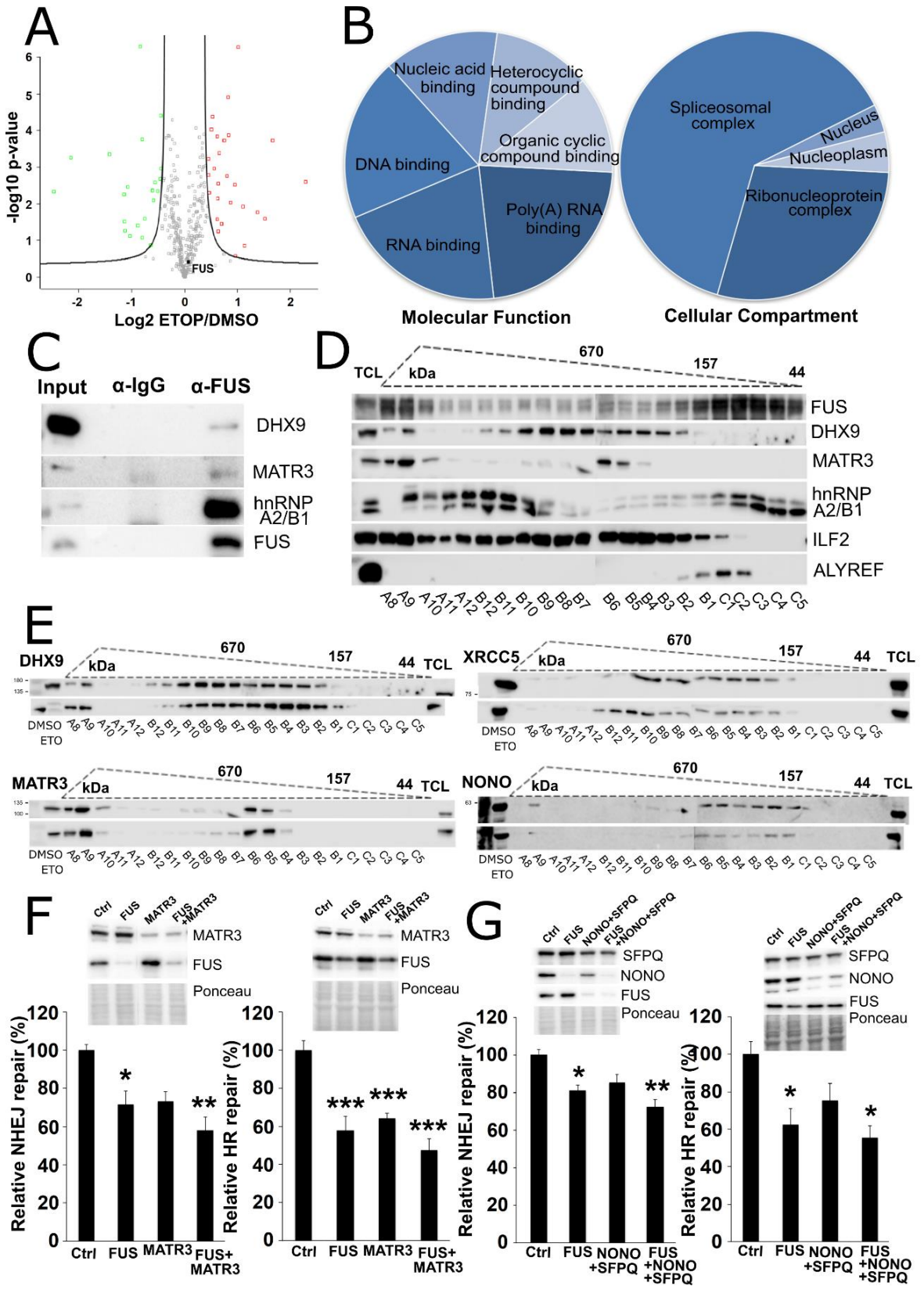

Figure 4. **Proteomic analysis of the FUS interactome.**

A. Representative Volcano-plot of the result of the t-test comparing the intensities of the common 432 proteins identified in ETO-treated and control immunoprecipitations. The log2 ratio between the averaged LFQ-intensities of the proteins identified in ETO versus control condition are plotted against

bioRxiv preprint doi: https://doi.org/10.1101/798884; this version posted October 11, 2019. The copyright holder for this preprint (which was not certified by peer review) is the author/funder. All rights reserved. No reuse allowed without permission.

the negative log10 p-value of the test, after a Benjamini-Hochberg false discovery rate correction; log2 ETO/DMSO indicates the ratio between the mean protein intensities; proteins with a log2 ratio ETOP/DMSO >0.5 were defined as "up regulated" (red square) or <0.5 were defined as "down regulated" (green square);

B. Gene Ontology Biological process analysis was performed on the FUS interactors with higher affinity for FUS upon etoposide treatment, according to molecular function (a) and cellular component (b) terms; the colour gradient indicates the fold change enrichment of the GO term in the dataset with respect to the human reference set. All terms are statistically significantly enriched with a p-value <0.05 (after Bonferroni correction for multiple testing).

C. Validation of FUS interactors by Western blotting with the indicated antibodies in the presence of RNase A. Arrow heads indicate the two isoforms of hnRNP A2B1.

D. Size exclusion chromatography of FUS containing complexes HEK-293T/Flag-FUS were lysed and FUS interactors were purified from the total cell extract by anti-flag IP. The elution was subsequently subjected to the gel filtration column separation. Fractions were analysed by Western blotting with the indicated antibodies. Fractions were analysed by Western blotting with the indicated antibodies. Fraction numbers and the positions of the molecular mass standards are indicated.

E. HEK293T/Flag-FUS were treated with 10 µM etoposide for 1 h (ETO) or DMSO as control. Immunoprecipitated complexes were analysed as in E.

F. DSBs repair efficiency upon depletion of MATR3 was quantified in U2OS cells containing a stably integrated NHEJ (left panel) or a HR (right panel) reporter system. The results were shown as mean ± SEM. from at least three biological repeats. Statistical analysis was performed by one-way ANOVA, which revealed a significant difference of HR repair ($F_{3,31}$=17.55, p<0.001) and of NHEJ ($F_{3,8}$=9.5, p=0.005). Data analysis was followed by Bonferroni post-hoc test. *p<0.05; **p<0.01; ***p<0.001. *Upper panels*: representative depletions of the indicated proteins. *Lower panels*: Quantification of relative repair efficiency.

G. DSBs repair efficiency upon depletion of SFPQ/NONO was quantified as in F. Statistical analysis was performed by one-way ANOVA, which revealed a significant difference of HR repair ($F_{3,16}$=5.46, p=0.009) and of NHEJ ($F_{3,8}$=11.09, p=0.003). Data analysis was followed by Bonferroni post-hoc test. *p<0.05; **p<0.01; ***p<0.001.

bioRxiv preprint doi: https://doi.org/10.1101/798884; this version posted October 11, 2019. The copyright holder for this preprint (which was not certified by peer review) is the author/funder. All rights reserved. No reuse allowed without permission.

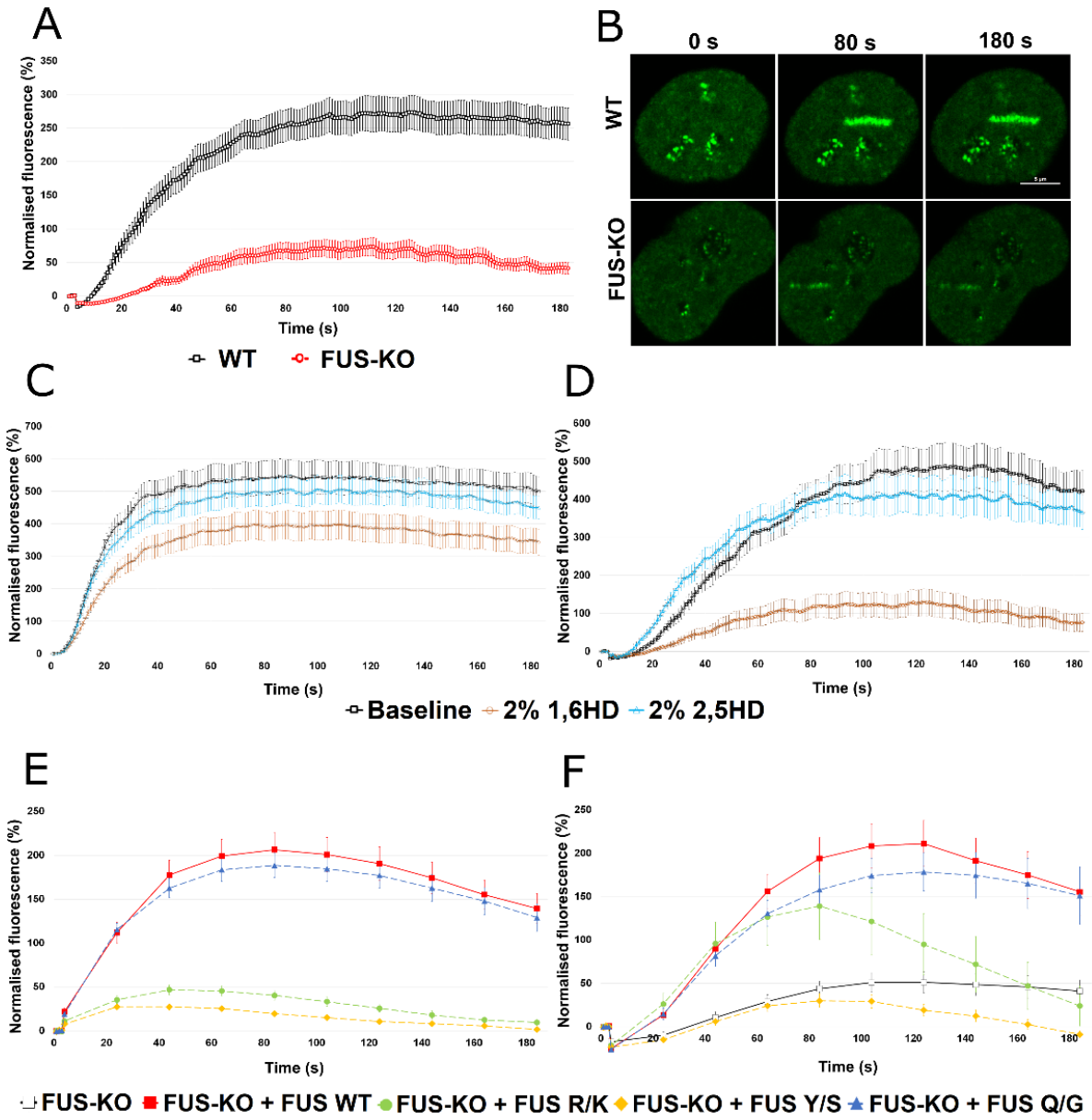

Figure 5. **SFPQ recruitment to DNA damage sites is dependent on FUS and on LLPS.**

A. WT HeLa and HeLa FUS-KO cells were transiently transfected with a GFP-SFPQ expressing plasmid and subjected to laser microirradiation as described in Figure 3D. Curve graphs show fluorescence intensities of GFP-fusion proteins at the irradiated region that were quantified periodically, normalised and presented as mean ± SEM for 10 cells in each experiment. Experiments were performed in duplicate.

B. Representative images of WT HeLa and HeLa FUS-KO cells were transiently transfected with a GFP-SFPQ expressing plasmid and subjected to laser microirradiation. Left panels show cells at baseline (before laser microirradiation). Middle panels show cells at the peak of recruitment (80 s after irradiation). Right panels show cells at the end of assessment (180 s after irradiation).

C. WT Hela cells were transiently transfected with a GFP-FUS expressing plasmid and incubated with either 2% 1,6 HD or 2% 2,5 HD for 30 minutes prior to laser microirradiation.

D. WT Hela cells were transiently transfected with a GFP-SFPQ expressing plasmid and treated as in B.

bioRxiv preprint doi: https://doi.org/10.1101/798884; this version posted October 11, 2019. The copyright holder for this preprint (which was not certified by peer review) is the author/funder. All rights reserved. No reuse allowed without permission.

E. HeLa FUS-KO cells were transiently transfected with constructs expressing WT FUS or the indicated variants fused to mCherry and then subjected to laser microirradiation. Curve graphs show fluorescence intensities of mCherry-fusion proteins at the irradiated region as in A.

F. HeLa FUS-KO cells were transiently transfected with a plasmid expressing GFP-SFPQ or co-transfected with GFP SFPQ and with constructs expressing the indicated FUS-mCherry variants prior to laser microirradiation. Curve graphs show fluorescence intensities of GFP-SFPQ at the irradiated region as in A.

bioRxiv preprint doi: https://doi.org/10.1101/798884; this version posted October 11, 2019. The copyright holder for this preprint (which was not certified by peer review) is the author/funder. All rights reserved. No reuse allowed without permission.

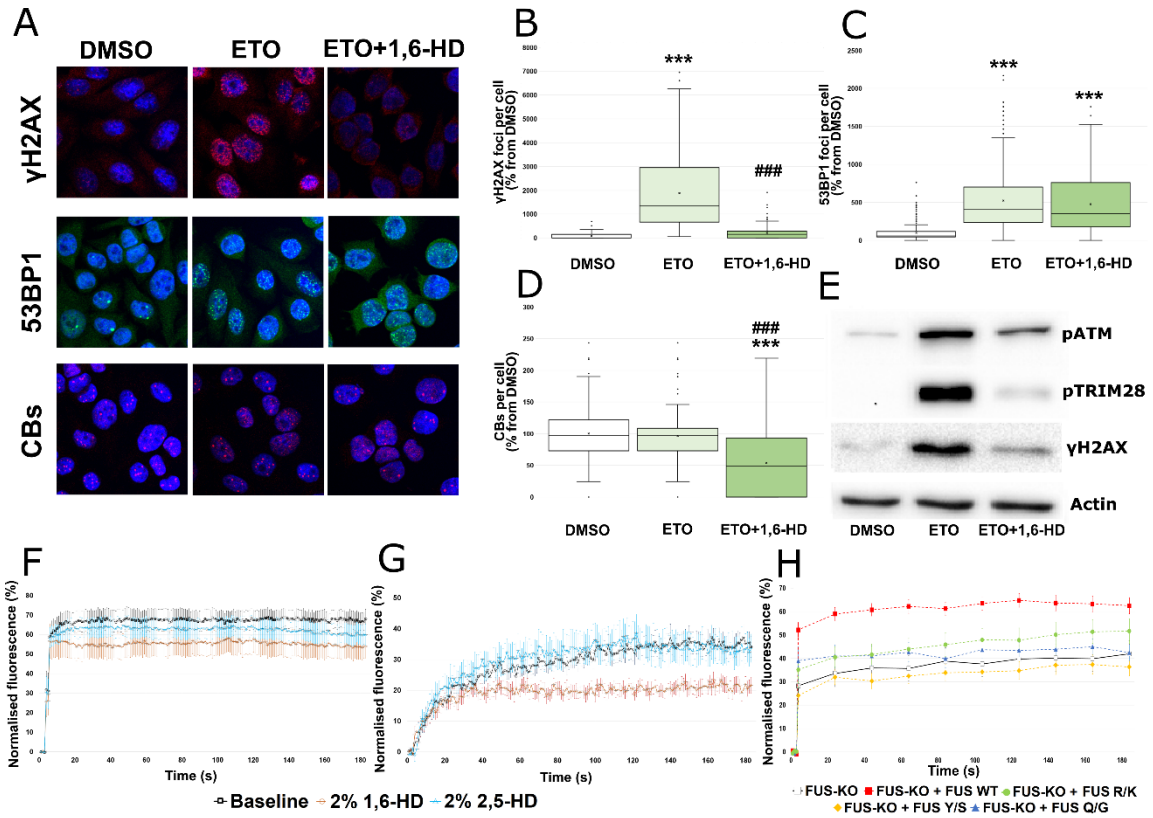

Figure 6. **Liquid-liquid phase transition is required for effective DDR and γH2AX foci formation.**

A. Representative confocal micrographs of HeLa that were treated with ETO alone or with ETO and 1,6 HD for 30 minutes prior to immunostaining for γH2AX (top three images), 53BP1 (middle three images) and Coilin (Cajal bodies – CBs, bottom three images) of cells. Scale bar represents 5 µm.

B. Quantification of γH2AX foci of the experiment described in A. Fluorescence intensities were scored with Image J. 200 cells were analysed per condition and experiments were performed in duplicates. One-way ANOVA revealed a significant effect of the treatments ($F_{2,1197}$=522.93, p<0.001). Data was further analysed by Bonferroni post hoc test was. ***p<0.001 in comparison to DMSO group; ###p<0.001 in comparison to ETO group.

C. Quantification of 53BP1 foci of the experiment described in Panel A. One-way ANOVA revealed a significant effect of the treatments ($F_{2,1197}$=201.58, p<0.001). Data was further analysed by Bonferroni post hoc test was. ***p<0.001 in comparison to DMSO group.

D. Quantification of Cajal Bodies – CBs (detected with coilin staining) of the experiment described in Panel A. One-way ANOVA revealed a significant effect of the treatments ($F_{2,1197}$=147.61, p<0.001). Data was further analysed by Bonferroni post hoc test was. ***p<0.001 in comparison to DMSO group; ###p<0.001 in comparison to ETO group.

E. Western blot analysis of total extracts prepared from HeLa cells that were treated as in Panel A. Actin was used as a normaliser.

F. WT Hela cells were transiently transfected with GFP-KU80 expressing plasmids and then incubated with either 2% 1,6 HD or 2% 2,5 HD for 30 minutes prior to laser microirradiation as in Figure 5C/D.

G. WT Hela cells were transiently transfected with GFP-NBS1 expressing plasmids and then incubated with either 2% 1,6 HD or 2% 2,5 HD for 30 minutes prior to laser microirradiation as in Figure 5C/D.

bioRxiv preprint doi: https://doi.org/10.1101/798884; this version posted October 11, 2019. The copyright holder for this preprint (which was not certified by peer review) is the author/funder. All rights reserved. No reuse allowed without permission.

H. HeLa FUS-KO cells were transiently co-transfected with a plasmid expressing GFP-KU80 and with constructs expressing the indicated FUS-mCherry variants prior to laser microirradiation. Curve graphs show fluorescence intensities of GFP-SFPQ at the irradiated region.

bioRxiv preprint doi: https://doi.org/10.1101/798884; this version posted October 11, 2019. The copyright holder for this preprint (which was not certified by peer review) is the author/funder. All rights reserved. No reuse allowed without permission.

References

Abbasi, S., and Schild-Poulter, C. (2018). Mapping the Ku interactome using proximity-dependent biotin identification in human cells. Journal of proteome research.

Akhmedov, A.T., and Lopez, B.S. (2000). Human 100-kDa homologous DNA-pairing protein is the splicing factor PSF and promotes DNA strand invasion. Nucleic acids research *28*, 3022-3030.

Aleksandrov, R., Dotchev, A., Poser, I., Krastev, D., Georgiev, G., Panova, G., Babukov, Y., Danovski, G., Dyankova, T., Hubatsch, L., *et al.* (2018). Protein Dynamics in Complex DNA Lesions. Molecular cell *69*, 1046-1061 e1045.

Baechtold, H., Kuroda, M., Sok, J., Ron, D., Lopez, B.S., and Akhmedov, A.T. (1999). Human 75-kDa DNA-pairing protein is identical to the pro-oncoprotein TLS/FUS and is able to promote D-loop formation. The Journal of biological chemistry *274*, 34337-34342.

Bladen, C.L., Udayakumar, D., Takeda, Y., and Dynan, W.S. (2005). Identification of the polypyrimidine tract binding protein-associated splicing factor.p54(nrb) complex as a candidate DNA double-strand break rejoining factor. The Journal of biological chemistry *280*, 5205-5210.

Boeynaems, S., Alberti, S., Fawzi, N.L., Mittag, T., Polymenidou, M., Rousseau, F., Schymkowitz, J., Shorter, J., Wolozin, B., Van Den Bosch, L., *et al.* (2018). Protein Phase Separation: A New Phase in Cell Biology. Trends in cell biology *28*, 420-435.

Boguslawski, S.J., Smith, D.E., Michalak, M.A., Mickelson, K.E., Yehle, C.O., Patterson, W.L., and Carrico, R.J. (1986). Characterization of monoclonal antibody to DNA.RNA and its application to immunodetection of hybrids. Journal of immunological methods *89*, 123-130.

Burke, K.A., Janke, A.M., Rhine, C.L., and Fawzi, N.L. (2015). Residue-by-Residue View of In Vitro FUS Granules that Bind the C-Terminal Domain of RNA Polymerase II. Molecular cell *60*, 231-241.

Cerritelli, S.M., Frolova, E.G., Feng, C., Grinberg, A., Love, P.E., and Crouch, R.J. (2003). Failure to produce mitochondrial DNA results in embryonic lethality in Rnaseh1 null mice. Mol Cell *11*, 807-815.

Chakraborty, P., Huang, J.T.J., and Hiom, K. (2018). DHX9 helicase promotes R-loop formation in cells with impaired RNA splicing. Nature communications *9*, 4346.

Chanut, P., Britton, S., Coates, J., Jackson, S.P., and Calsou, P. (2016). Coordinated nuclease activities counteract Ku at single-ended DNA double-strand breaks. Nature communications *7*, 12889.

Chia, R., Chio, A., and Traynor, B.J. (2018). Novel genes associated with amyotrophic lateral sclerosis: diagnostic and clinical implications. The Lancet. Neurology *17*, 94-102.

Chuang, T.W., Lu, C.C., Su, C.H., Wu, P.Y., Easwvaran, S., Lee, C.C., Kuo, H.C., Hung, K.Y., Lee, K.M., Tsai, C.Y., *et al.* (2019). The RNA Processing Factor Y14 Participates in DNA Damage Response and Repair. iScience *13*, 402-415.

bioRxiv preprint doi: https://doi.org/10.1101/798884; this version posted October 11, 2019. The copyright holder for this preprint (which was not certified by peer review) is the author/funder. All rights reserved. No reuse allowed without permission.

Cox, J., Neuhauser, N., Michalski, A., Scheltema, R.A., Olsen, J.V., and Mann, M. (2011). Andromeda: a peptide search engine integrated into the MaxQuant environment. Journal of proteome research *10*, 1794-1805.

Cristini, A., Groh, M., Kristiansen, M.S., and Gromak, N. (2018). RNA/DNA Hybrid Interactome Identifies DXH9 as a Molecular Player in Transcriptional Termination and R-Loop-Associated DNA Damage. Cell reports *23*, 1891-1905.

Deng, Q., Holler, C.J., Taylor, G., Hudson, K.F., Watkins, W., Gearing, M., Ito, D., Murray, M.E., Dickson, D.W., Seyfried, N.T., *et al.* (2014). FUS is phosphorylated by DNA-PK and accumulates in the cytoplasm after DNA damage. The Journal of neuroscience : the official journal of the Society for Neuroscience *34*, 7802-7813.

Dormann, D., and Haass, C. (2013). Fused in sarcoma (FUS): an oncogene goes awry in neurodegeneration. Molecular and cellular neurosciences *56*, 475-486.

Francia, S., Michelini, F., Saxena, A., Tang, D., de Hoon, M., Anelli, V., Mione, M., Carninci, P., and d'Adda di Fagagna, F. (2012). Site-specific DICER and DROSHA RNA products control the DNA-damage response. Nature *488*, 231-235.

Gardiner, M., Toth, R., Vandermoere, F., Morrice, N.A., and Rouse, J. (2008). Identification and characterization of FUS/TLS as a new target of ATM. The Biochemical journal *415*, 297-307.

Gunn, A., and Stark, J.M. (2012). I-SceI-based assays to examine distinct repair outcomes of mammalian chromosomal double strand breaks. Methods in molecular biology (Clifton, N.J.) *920*, 379-391.

Harrison, A.F., and Shorter, J. (2017). RNA-binding proteins with prion-like domains in health and disease. The Biochemical journal *474*, 1417-1438.

Hennig, S., Kong, G., Mannen, T., Sadowska, A., Kobelke, S., Blythe, A., Knott, G.J., Iyer, K.S., Ho, D., Newcombe, E.A., *et al.* (2015). Prion-like domains in RNA binding proteins are essential for building subnuclear paraspeckles. The Journal of cell biology *210*, 529-539.

Hicks, G.G., Singh, N., Nashabi, A., Mai, S., Bozek, G., Klewes, L., Arapovic, D., White, E.K., Koury, M.J., Oltz, E.M., *et al.* (2000). Fus deficiency in mice results in defective B-lymphocyte development and activation, high levels of chromosomal instability and perinatal death. Nature genetics *24*, 175-179.

Hill, S.J., Mordes, D.A., Cameron, L.A., Neuberg, D.S., Landini, S., Eggan, K., and Livingston, D.M. (2016). Two familial ALS proteins function in prevention/repair of transcription-associated DNA damage. Proceedings of the National Academy of Sciences of the United States of America *113*, E7701-E7709.

Hirose, T., Yamazaki, T., and Nakagawa, S. (2019). Molecular anatomy of the architectural NEAT1 noncoding RNA: The domains, interactors, and biogenesis pathway required to build phase-separated nuclear paraspeckles. Wiley interdisciplinary reviews. RNA, e1545.

Jaafar, L., Li, Z., Li, S., and Dynan, W.S. (2017). SFPQ*NONO and XLF function separately and together to promote DNA double-strand break repair via canonical nonhomologous end joining. Nucleic acids research *45*, 1848-1859.

bioRxiv preprint doi: https://doi.org/10.1101/798884; this version posted October 11, 2019. The copyright holder for this preprint (which was not certified by peer review) is the author/funder. All rights reserved. No reuse allowed without permission.

Kato, M., Han, T.W., Xie, S., Shi, K., Du, X., Wu, L.C., Mirzaei, H., Goldsmith, E.J., Longgood, J., Pei, J., *et al.* (2012). Cell-free formation of RNA granules: low complexity sequence domains form dynamic fibers within hydrogels. Cell *149*, 753-767.

Kroschwald, S., Maharana, S., Mateju, D., Malinovska, L., Nuske, E., Poser, I., Richter, D., and Alberti, S. (2015). Promiscuous interactions and protein disaggregases determine the material state of stress-inducible RNP granules. eLife *4*, e06807.

Kruhlak, M.J., Celeste, A., Dellaire, G., Fernandez-Capetillo, O., Muller, W.G., McNally, J.G., Bazett-Jones, D.P., and Nussenzweig, A. (2006). Changes in chromatin structure and mobility in living cells at sites of DNA double-strand breaks. The Journal of cell biology *172*, 823-834.

Kuhnert, A., Schmidt, U., Monajembashi, S., Franke, C., Schlott, B., Grosse, F., Greulich, K.O., Saluz, H.P., and Hanel, F. (2012). Proteomic identification of PSF and p54(nrb) as TopBP1-interacting proteins. Journal of cellular biochemistry *113*, 1744-1753.

Kuroda, M., Sok, J., Webb, L., Baechtold, H., Urano, F., Yin, Y., Chung, P., de Rooij, D.G., Akhmedov, A., Ashley, T., *et al.* (2000). Male sterility and enhanced radiation sensitivity in TLS(-/-) mice. The EMBO journal *19*, 453-462.

Lee, M., Sadowska, A., Bekere, I., Ho, D., Gully, B.S., Lu, Y., Iyer, K.S., Trewhella, J., Fox, A.H., and Bond, C.S. (2015). The structure of human SFPQ reveals a coiled-coil mediated polymer essential for functional aggregation in gene regulation. Nucleic acids research *43*, 3826-3840.

Li, X., and Manley, J.L. (2005). Inactivation of the SR protein splicing factor ASF/SF2 results in genomic instability. Cell *122*, 365-378.

Li, X., Wang, J., and Manley, J.L. (2005). Loss of splicing factor ASF/SF2 induces G2 cell cycle arrest and apoptosis, but inhibits internucleosomal DNA fragmentation. Genes & development *19*, 2705-2714.

Lin, Y., Mori, E., Kato, M., Xiang, S., Wu, L., Kwon, I., and McKnight, S.L. (2016). Toxic PR Poly-Dipeptides Encoded by the C9orf72 Repeat Expansion Target LC Domain Polymers. Cell *167*, 789-802 e712.

Marchesini, M., Ogoti, Y., Fiorini, E., Aktas Samur, A., Nezi, L., D'Anca, M., Storti, P., Samur, M.K., Ganan-Gomez, I., Fulciniti, M.T., *et al.* (2017). ILF2 Is a Regulator of RNA Splicing and DNA Damage Response in 1q21-Amplified Multiple Myeloma. Cancer cell *32*, 88-100 e106.

Mastrocola, A.S., Kim, S.H., Trinh, A.T., Rodenkirch, L.A., and Tibbetts, R.S. (2013). The RNA-binding protein fused in sarcoma (FUS) functions downstream of poly(ADP-ribose) polymerase (PARP) in response to DNA damage. The Journal of biological chemistry *288*, 24731-24741.

Matsuoka, S., Ballif, B.A., Smogorzewska, A., McDonald, E.R., 3rd, Hurov, K.E., Luo, J., Bakalarski, C.E., Zhao, Z., Solimini, N., Lerenthal, Y., *et al.* (2007). ATM and ATR substrate analysis reveals extensive protein networks responsive to DNA damage. Science (New York, N.Y.) *316*, 1160-1166.

Michelini, F., Pitchiaya, S., Vitelli, V., Sharma, S., Gioia, U., Pessina, F., Cabrini, M., Wang, Y., Capozzo, I., Iannelli, F., *et al.* (2017). Damage-induced lncRNAs control the

bioRxiv preprint doi: https://doi.org/10.1101/798884; this version posted October 11, 2019. The copyright holder for this preprint (which was not certified by peer review) is the author/funder. All rights reserved. No reuse allowed without permission.

DNA damage response through interaction with DDRNAs at individual double-strand breaks. Nature cell biology *19*, 1400-1411.

Mikolaskova, B., Jurcik, M., Cipakova, I., Kretova, M., Chovanec, M., and Cipak, L. (2018). Maintenance of genome stability: the unifying role of interconnections between the DNA damage response and RNA-processing pathways. Current genetics *64*, 971-983.

Molliex, A., Temirov, J., Lee, J., Coughlin, M., Kanagaraj, A.P., Kim, H.J., Mittag, T., and Taylor, J.P. (2015). Phase separation by low complexity domains promotes stress granule assembly and drives pathological fibrillization. Cell *163*, 123-133.

Morchikh, M., Cribier, A., Raffel, R., Amraoui, S., Cau, J., Severac, D., Dubois, E., Schwartz, O., Bennasser, Y., and Benkirane, M. (2017). HEXIM1 and NEAT1 Long Non-coding RNA Form a Multi-subunit Complex that Regulates DNA-Mediated Innate Immune Response. Molecular cell *67*, 387-399 e385.

Moumen, A., Magill, C., Dry, K.L., and Jackson, S.P. (2013). ATM-dependent phosphorylation of heterogeneous nuclear ribonucleoprotein K promotes p53 transcriptional activation in response to DNA damage. Cell cycle (Georgetown, Tex.) *12*, 698-704.

Murakami, T., Qamar, S., Lin, J.Q., Schierle, G.S., Rees, E., Miyashita, A., Costa, A.R., Dodd, R.B., Chan, F.T., Michel, C.H., *et al.* (2015). ALS/FTD Mutation-Induced Phase Transition of FUS Liquid Droplets and Reversible Hydrogels into Irreversible Hydrogels Impairs RNP Granule Function. Neuron *88*, 678-690.

Myler, L.R., Gallardo, I.F., Soniat, M.M., Deshpande, R.A., Gonzalez, X.B., Kim, Y., Paull, T.T., and Finkelstein, I.J. (2017). Single-Molecule Imaging Reveals How Mre11-Rad50-Nbs1 Initiates DNA Break Repair. Molecular cell *67*, 891-898 e894.

Naganuma, T., Nakagawa, S., Tanigawa, A., Sasaki, Y.F., Goshima, N., and Hirose, T. (2012). Alternative 3'-end processing of long noncoding RNA initiates construction of nuclear paraspeckles. The EMBO journal *31*, 4020-4034.

Ohle, C., Tesorero, R., Schermann, G., Dobrev, N., Sinning, I., and Fischer, T. (2016). Transient RNA-DNA Hybrids Are Required for Efficient Double-Strand Break Repair. Cell *167*, 1001-1013 e1007.

Patel, A., Lee, H.O., Jawerth, L., Maharana, S., Jahnel, M., Hein, M.Y., Stoynov, S., Mahamid, J., Saha, S., Franzmann, T.M., *et al.* (2015). A Liquid-to-Solid Phase Transition of the ALS Protein FUS Accelerated by Disease Mutation. Cell *162*, 1066-1077.

Paulsen, R.D., Soni, D.V., Wollman, R., Hahn, A.T., Yee, M.C., Guan, A., Hesley, J.A., Miller, S.C., Cromwell, E.F., Solow-Cordero, D.E., *et al.* (2009). A genome-wide siRNA screen reveals diverse cellular processes and pathways that mediate genome stability. Molecular cell *35*, 228-239.

Pessina, F., Giavazzi, F., Yin, Y., Gioia, U., Vitelli, V., Galbiati, A., Barozzi, S., Garre, M., Oldani, A., Flaus, A., *et al.* (2019). Functional transcription promoters at DNA double-strand breaks mediate RNA-driven phase separation of damage-response factors. Nature cell biology.

bioRxiv preprint doi: https://doi.org/10.1101/798884; this version posted October 11, 2019. The copyright holder for this preprint (which was not certified by peer review) is the author/funder. All rights reserved. No reuse allowed without permission.

Petti, E., Buemi, V., Zappone, A., Schillaci, O., Broccia, P.V., Dinami, R., Matteoni, S., Benetti, R., and Schoeftner, S. (2019). SFPQ and NONO suppress RNA:DNA-hybrid-related telomere instability. Nature communications *10*, 1001.

Polo, S.E., Blackford, A.N., Chapman, J.R., Baskcomb, L., Gravel, S., Rusch, A., Thomas, A., Blundred, R., Smith, P., Kzhyshkowska, J., *et al.* (2012). Regulation of DNA-end resection by hnRNPU-like proteins promotes DNA double-strand break signaling and repair. Molecular cell *45*, 505-516.

Rajesh, C., Baker, D.K., Pierce, A.J., and Pittman, D.L. (2011). The splicing-factor related protein SFPQ/PSF interacts with RAD51D and is necessary for homology-directed repair and sister chromatid cohesion. Nucleic acids research *39*, 132-145.

Rappsilber, J., Mann, M., and Ishihama, Y. (2007). Protocol for micro-purification, enrichment, pre-fractionation and storage of peptides for proteomics using StageTips. Nature protocols *2*, 1896-1906.

Reber, S., Mechtersheimer, J., Nasif, S., Benitez, J.A., Colombo, M., Domanski, M., Jutzi, D., Hedlund, E., and Ruepp, M.D. (2018). CRISPR-Trap: a clean approach for the generation of gene knockouts and gene replacements in human cells. Molecular biology of the cell *29*, 75-83.

Reber, S., Stettler, J., Filosa, G., Colombo, M., Jutzi, D., Lenzken, S.C., Schweingruber, C., Bruggmann, R., Bachi, A., Barabino, S.M., *et al.* (2016). Minor intron splicing is regulated by FUS and affected by ALS-associated FUS mutants. The EMBO journal *35*, 1504-1521.

Rogelj, B., Easton, L.E., Bogu, G.K., Stanton, L.W., Rot, G., Curk, T., Zupan, B., Sugimoto, Y., Modic, M., Haberman, N., *et al.* (2012). Widespread binding of FUS along nascent RNA regulates alternative splicing in the brain. Scientific reports *2*, 603.

Salton, M., Lerenthal, Y., Wang, S.Y., Chen, D.J., and Shiloh, Y. (2010). Involvement of Matrin 3 and SFPQ/NONO in the DNA damage response. Cell cycle (Georgetown, Tex.) *9*, 1568-1576.

Shen, W., Sun, H., De Hoyos, C.L., Bailey, J.K., Liang, X.H., and Crooke, S.T. (2017). Dynamic nucleoplasmic and nucleolar localization of mammalian RNase H1 in response to RNAP I transcriptional R-loops. Nucleic acids research *45*, 10672-10692.

Shibata, A., Jeggo, P., and Lobrich, M. (2018). The pendulum of the Ku-Ku clock. DNA repair.

Simon, N.E., Yuan, M., and Kai, M. (2017). RNA-binding protein RBM14 regulates dissociation and association of non-homologous end joining proteins. Cell cycle (Georgetown, Tex.) *16*, 1175-1180.

Singatulina, A.S., Hamon, L., Sukhanova, M.V., Desforges, B., Joshi, V., Bouhss, A., Lavrik, O.I., and Pastre, D. (2019). PARP-1 Activation Directs FUS to DNA Damage Sites to Form PARG-Reversible Compartments Enriched in Damaged DNA. Cell reports *27*, 1809-1821 e1805.

Sollier, J., Stork, C.T., Garcia-Rubio, M.L., Paulsen, R.D., Aguilera, A., and Cimprich, K.A. (2014). Transcription-coupled nucleotide excision repair factors promote R-loop-induced genome instability. Molecular cell *56*, 777-785.

bioRxiv preprint doi: https://doi.org/10.1101/798884; this version posted October 11, 2019. The copyright holder for this preprint (which was not certified by peer review) is the author/funder. All rights reserved. No reuse allowed without permission.

Stirling, P.C., Chan, Y.A., Minaker, S.W., Aristizabal, M.J., Barrett, I., Sipahimalani, P., Kobor, M.S., and Hieter, P. (2012). R-loop-mediated genome instability in mRNA cleavage and polyadenylation mutants. Genes & development *26*, 163-175.

Stucki, M., and Jackson, S.P. (2006). gammaH2AX and MDC1: anchoring the DNA-damage-response machinery to broken chromosomes. DNA repair *5*, 534-543.

Sui, J., Lin, Y.F., Xu, K., Lee, K.J., Wang, D., and Chen, B.P. (2015). DNA-PKcs phosphorylates hnRNP-A1 to facilitate the RPA-to-POT1 switch and telomere capping after replication. Nucleic acids research *43*, 5971-5983.

Sun, Z., Diaz, Z., Fang, X., Hart, M.P., Chesi, A., Shorter, J., and Gitler, A.D. (2011). Molecular determinants and genetic modifiers of aggregation and toxicity for the ALS disease protein FUS/TLS. PLoS biology *9*, e1000614.

Updike, D.L., Hachey, S.J., Kreher, J., and Strome, S. (2011). P granules extend the nuclear pore complex environment in the C. elegans germ line. The Journal of Cell Biology *192*, 939-948.

Wahba, L., Amon, J.D., Koshland, D., and Vuica-Ross, M. (2011). RNase H and multiple RNA biogenesis factors cooperate to prevent RNA:DNA hybrids from generating genome instability. Molecular cell *44*, 978-988.

Wang, J., Choi, J.M., Holehouse, A.S., Lee, H.O., Zhang, X., Jahnel, M., Maharana, S., Lemaitre, R., Pozniakovsky, A., Drechsel, D., *et al.* (2018). A Molecular Grammar Governing the Driving Forces for Phase Separation of Prion-like RNA Binding Proteins. Cell *174*, 688-699 e616.

Wang, W.Y., Pan, L., Su, S.C., Quinn, E.J., Sasaki, M., Jimenez, J.C., Mackenzie, I.R., Huang, E.J., and Tsai, L.H. (2013). Interaction of FUS and HDAC1 regulates DNA damage response and repair in neurons. Nature neuroscience *16*, 1383-1391.

Wisniewski, J.R. (2017). Filter-Aided Sample Preparation: The Versatile and Efficient Method for Proteomic Analysis. Methods in enzymology *585*, 15-27.

Yamaguchi, A., and Takanashi, K. (2016). FUS interacts with nuclear matrix-associated protein SAFB1 as well as Matrin3 to regulate splicing and ligand-mediated transcription. Scientific reports *6*, 35195.

Yamazaki, T., Souquere, S., Chujo, T., Kobelke, S., Chong, Y.S., Fox, A.H., Bond, C.S., Nakagawa, S., Pierron, G., and Hirose, T. (2018). Functional Domains of NEAT1 Architectural lncRNA Induce Paraspeckle Assembly through Phase Separation. Molecular cell *70*, 1038-1053 e1037.

Yu, Y., and Reed, R. (2015). FUS functions in coupling transcription to splicing by mediating an interaction between RNAP II and U1 snRNP. Proceedings of the National Academy of Sciences of the United States of America *112*, 8608-8613.